1 Introduction

1.1 Bravais Lattice and Reciprocal Lattice

A fundamental concept in the description of any crystal is the Bravais lattice, which specifies the periodic array in which the repeated unit cells of the crystal arranged. The units themselves may consist of single atoms, groups of atoms, or molecules but it is the Bravais lattice, which specifies the geometry of the underlying structure. A Bravais lattice is defined as an infinite array of discrete points with an arrangement and orientation. The array appears exactly the same, from whichever point the array is viewed. A Bravais lattice can be understood to consist of all the points with the position vectors:

$$\vec{R} = n_1\vec{a}_1 + n_2\vec{a}_2 + n_3\vec{a}_3$$

where, $\vec{a}_1, \vec{a}_2, \text{and}\, \vec{a}_3$ are called the primitive vectors of the Bravais lattice. Such a definition of Bravais lattice is general enough and can be used towards two or single dimensional structures too. By definition, since every point in the Bravais lattice is equivalent, the Bravais lattice must be infinite. Real crystal on the other hand are finite but are large enough so that every point, except at the surface, is equivalent. Real crystals can still be understood in terms of Bravais lattice as filling up only a finite portion of the entire lattice.

Primitive unit cell of a crystal is the fundamental unit of the crystal, when translated through the entire Bravais lattice vectors fills up the entire crystal without any overlap or voids. As shown in figure 1-1 the choice of the primitive unit cell is not unique. Conventional unit cells or simply units cells on the other hand can be larger than the primitive unit cell. A conventional unit cell is defined as the unit of the crystal which when translated with a subset of the Bravais lattice produces the entire crystal without any overlap. As mentioned before the conventional unit cell is larger than the primitive cell but illustrates the symmetry and the geometry of the crystal better.

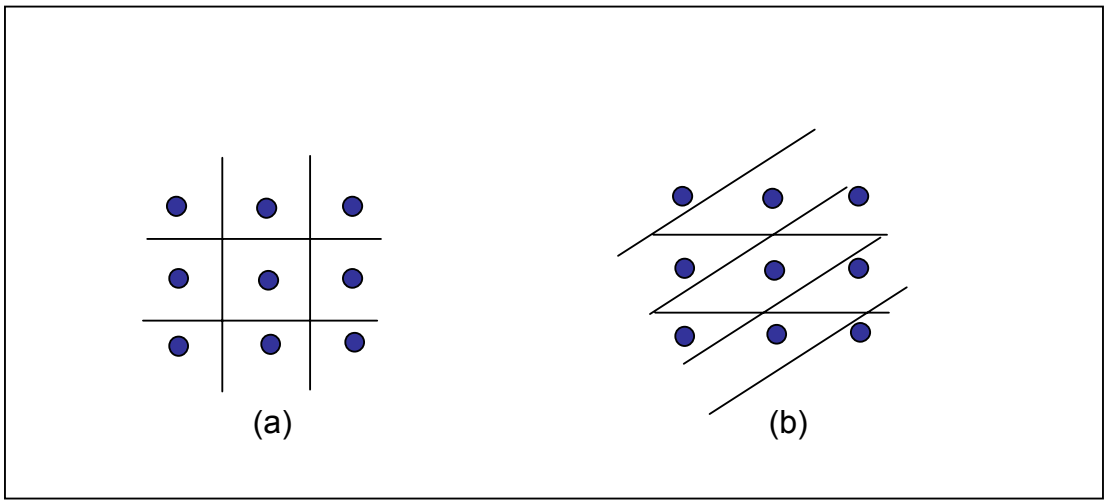

Figure 1-1 Different choice of unit cells for a crystal

The concept of reciprocal lattice is a very powerful and unavoidable tool used by crystallographer. One is led to it from very diverse avenues such as crystal diffraction, study of wave propagation in solids and band structure of solids.

Consider a set of points $\{\vec{R}\}$ belonging to a Bravais lattice such that $\vec{R} = n_1\vec{a}_1 + n_2\vec{a}_2 + n_3\vec{a}_3$, and a plane wave $e^{i.\vec{K}\cdot\vec{r}}$. The set of all wave vectors that yield a plane wave with the same periodicity as the Bravais lattice itself must satisfy the condition

$$e^{i\vec{K}\cdot(\vec{r}+\vec{R})} = e^{i\vec{K}\cdot\vec{r}} \Rightarrow e^{i\vec{K}\cdot\vec{R}} = 1 \Rightarrow \vec{K}\cdot\vec{R} = 2n\pi$$

The set of such wave vectors $\{\vec{K}\}$ is an array, where every vector of the array can be written as:

$$\vec{K} = k_1\vec{b}_1 + k_2\vec{b}_2 + k_3\vec{b}_3$$

Where

$$\vec{b}_1 = 2\pi\frac{\vec{a}_2 x\vec{a}_3}{\vec{a}_1\cdot(\vec{a}_2 x\vec{a}_3)}$$

$$\vec{b}_2 = 2\pi\frac{\vec{a}_3 x\vec{a}_1}{\vec{a}_1\cdot(\vec{a}_2 x\vec{a}_3)}$$

$$\vec{b}_3 = 2\pi\frac{\vec{a}_1 x\vec{a}_2}{\vec{a}_1\cdot(\vec{a}_2 x\vec{a}_3)}$$

The array of points satisfying the above conditions for a Bravais lattice by themselves and this lattice is called the reciprocal lattice. In the next section the flexibility and power of this concept will be evident when x-ray diffraction from crystals is discussed. It should be noted that the reciprocal lattice has all the information and symmetry of the original lattice.

In defining the Bravais lattice only the translational symmetry of the crystal was exploited. These translational symmetries are by far the most important for the general theory of solids. Nonetheless crystal structures show other kind of symmetries too namely rotational and mirror symmetry, which are not included in Bravais lattice. Bravais lattice is characterized by the specification of all the operations that take the crystal into itself. This set of operations is called the symmetry group or space group of the Bravais lattice. The space group of a Bravais lattice includes all translations through lattice vector. In addition the space group includes all the rotational and mirrors operations that take the lattice into itself. The space group of a cubic Bravais lattice for example may include rotations though 90^o about a line of lattice points in the <100> direction.

Figure 1-2 illustrates this rotational operation. Rotating the lattice by 90^o (or an integral multiple of it) take the cubic lattice into itself. The <hkl> direction in crystallographic terms is the direction along the lattice vector

$$\vec{D}_{<hkl>} = h\vec{a}_1 + k\vec{a}_2 + l\vec{a}_3$$

The different possible operations that are included in a symmetry group of a Bravais lattice are

1. **Rotation through integral multiple of 2π/n about an axis**. This axis is then known as the n-fold rotation axis. (Bravais lattice can contain only 2, 3, 4, and 6 fold axis)
2. **Rotation-Reflection**. Even though in some cases a rotation may not be a symmetry operation, but rotation followed by a reflection in a plane perpendicular to the rotation axis may be. This axis is then called the rotation-reflection axis.
3. **Rotation-Inversion**. Similarly sometimes rotation followed by inversion ($\vec{R} \rightarrow -\vec{R}$) may be a symmetry operation of the Bravais lattice.

4. **Reflection**. Reflection about a plane can be a symmetry operation of the Bravais lattice in which case this plane is known as the mirror plane.
5. **Inversion**. Inversion (or reflection about the origin) can take the lattice into itself. In such a case inversion is an operation of the symmetry group of the lattice.

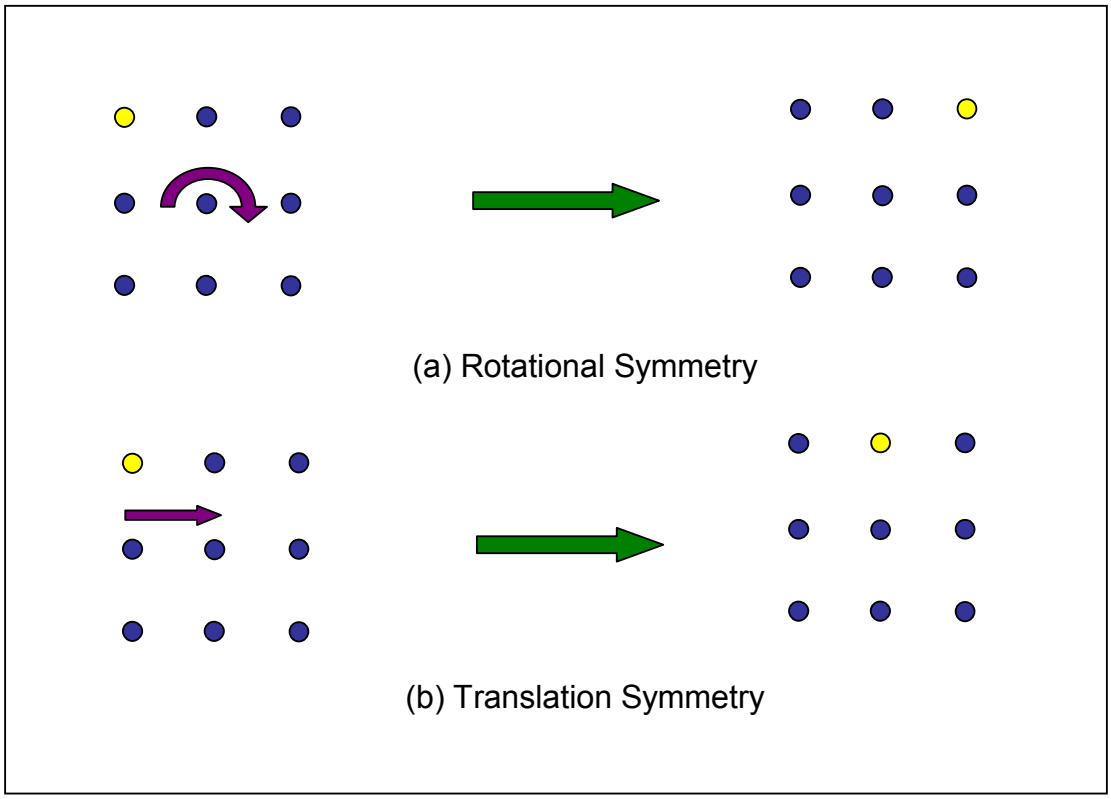

Figure 1-2 Symmetry operation of a cubic Bravais lattice

1.2 Crystal Structure of Silicon

In view of the fact that this study focuses on the structure of silicon surfaces and their phase transitions at high temperature, we introduce the crystalline structure of pure silicon. The lattice of pure silicon is the same as that of the diamond as shown in figure 1-3(c). To understand this lattice it is important to understand the Face Centered Cubic lattice. A cubic Bravais lattice is defined by three primitive vectors, which are equal in magnitude and orthogonal to each other as shown in figure 1-3(a). A Face Centered Cubic (FCC) lattice can be

derived from the cubic lattice by adding an atom to the center of each cubic face figure 1-3(b).

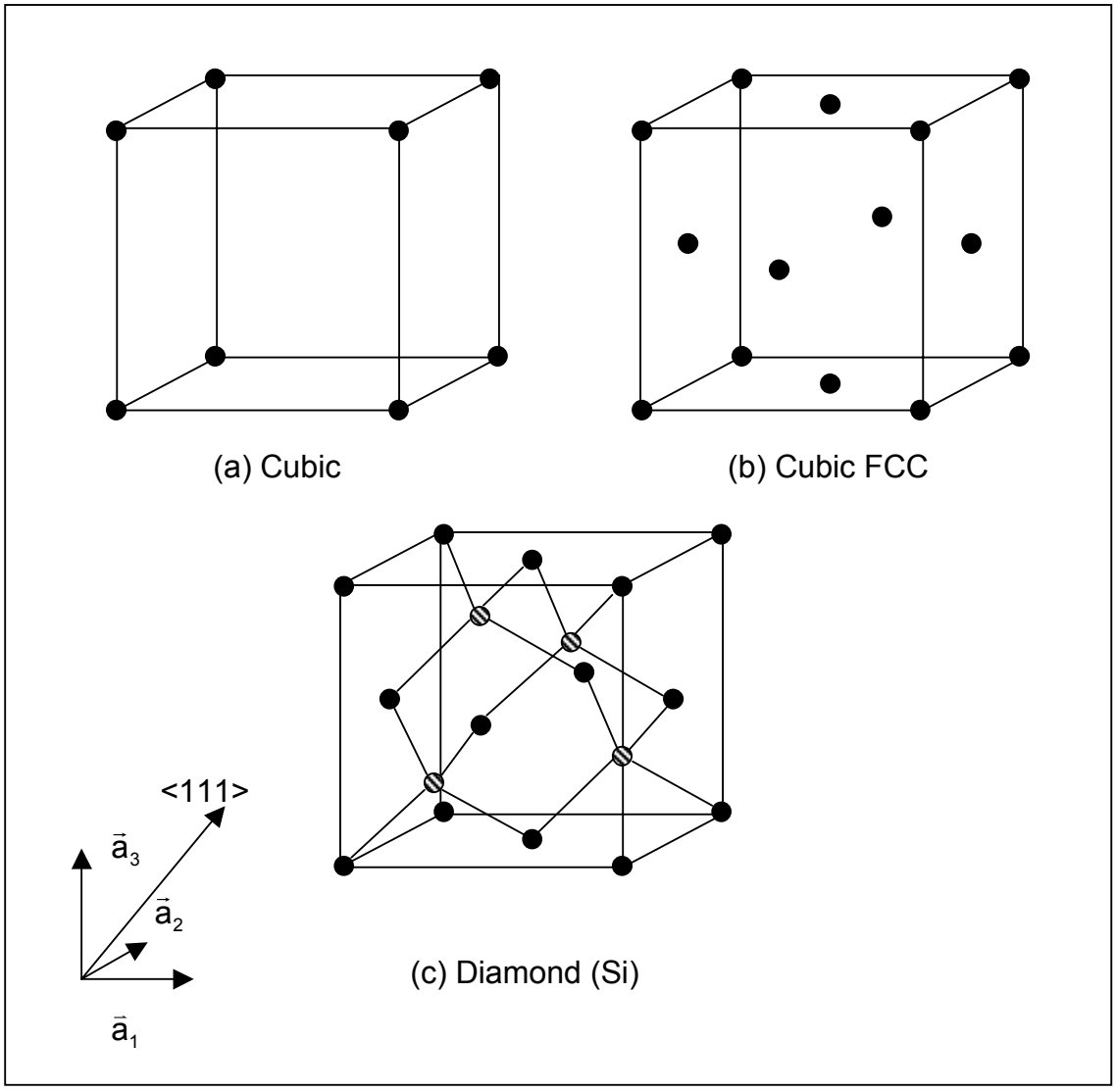

Figure 1-3 Cubic FCC and Diamond structures

The symmetry group of the Si crystal (diamond structure) can be better understood when viewed from the <111> direction. The unit cell of Si and its symmetry are shown in figure 1-4 when viewed from the <111> direction. The unit cell has a threefold symmetry along the <111> direction, therefore can be better represented by a hexagonal coordinate system. In terms of the hexagonal coordinate system unit cell of Si has a three-fold symmetry axis about the origin. The unit cell also has a mirror plane along the (2,1) direction.

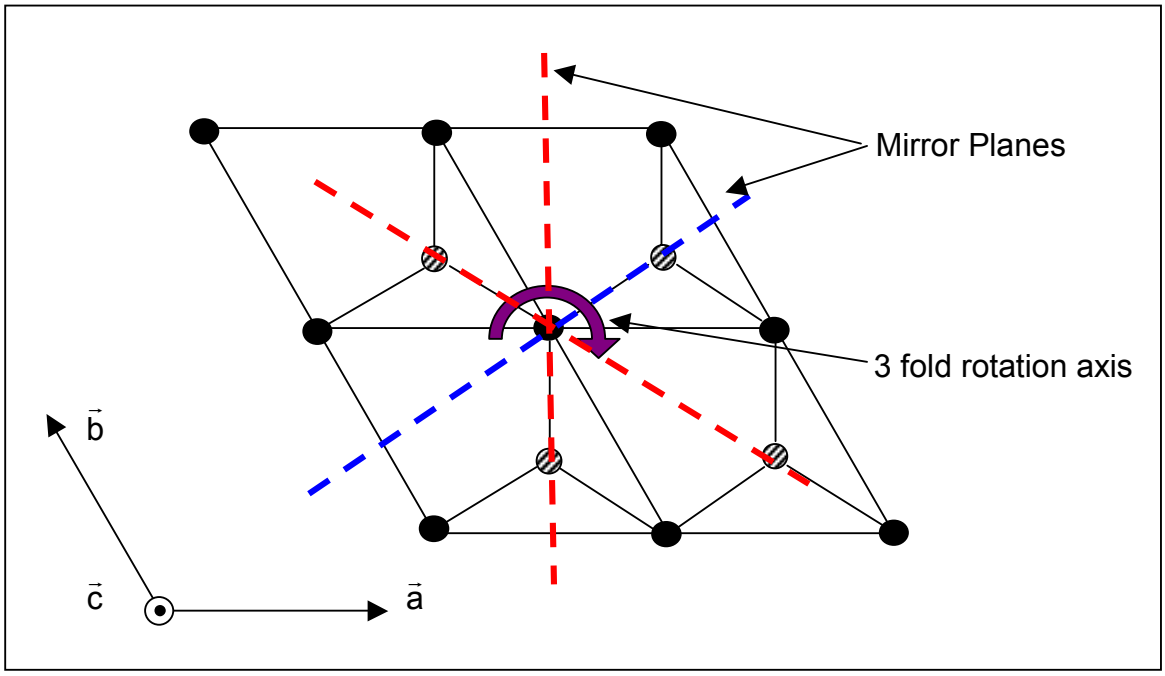

Figure 1-4 Unit cell and symmetry group of Si (111)

The 3 fold rotational symmetry produces two more mirror planes as shown in figure 1-4, but since these operation can be viewed as products of two operation (a rotation and a mirror operation) they are not considered as the fundamental operators of the symmetry group. This symmetry group of Si is called p3m1 indicating a three fold rotational axis and a mirror plane.

1.3 X-ray Diffraction

X-ray diffraction has been one of the mostly widely used methods for studying crystallographic structures for several decades now. Typical interatomic distances in a solid are on the order of an angstrom (10^{-8} cm). An electromagnetic probe of the microscopic structure of a solid must therefore have wavelength at least this short, corresponding to energies of the order

$$\hbar\omega = \frac{2\pi\hbar c}{\lambda} = \frac{2\pi\hbar\, c}{10^{-8}\,\mathrm{cm}} = 12.3\mathrm{X}10^{3}\,\mathrm{eV}$$

Such energies are characteristic of x-rays making them a suitable electromagnetic probe for studying the atomic structures of crystals. Crystalline solids show remarkable characteristic patterns of reflected x-ray unlike liquids

and amorphous solids. These patterns, commonly known as x-ray diffraction pattern are strongly dependent on the wavelength of the incident radiation and the angle of diffraction (angle between the wave vector of the incident beam and the reflected beam). When x-ray is incident on an atom of the crystal its predominant interaction is with the electrons of the atoms esp. the electrons in the valence shell. To understand this behavior of crystalline solids it is important to know what happens when x-ray interacts with electrons.

The interaction between x-rays and electrons is modeled quite accurately by the Thompson scattering formula. The Thompson scattering related the amplitude and the wave vector of the incident beam and the reflected beam by the formula

$$A_r \, \mathbf{exp(}-i\vec{k}_r \cdot \vec{r}\mathbf{)} = A_i \frac{e^2}{mc^2}\frac{1}{R_o}\mathbf{exp(}-i\vec{k}_i \cdot \vec{r}\mathbf{)}$$

$$A_r = A_i \frac{e^2}{mc^2}\frac{1}{R_o}\mathbf{exp(}-i(\vec{k}_i - \vec{k}_r)\cdot \vec{r}\mathbf{)}$$

In the above equation A_r, and A_i are the amplitudes of the reflected and incident waves, $\vec{r}$ is the position of the electron and $\vec{k}_i, \vec{k}_r$ are the incident and reflected wave vectors. The $\frac{1}{R_o}$ term is due to the fact that plane waves, upon scattered, gives rise to spherical waves as shown in figure 1-5.

The scattering is elastic if the energy of the incident plane wave is same as the energy of the reflected spherical wave, i.e. $\left|\vec{k}_i\right| = \left|\vec{k}_r\right| = \frac{2\pi}{\lambda}$. For elastic scattering the magnitude of the momentum transfer vector ($\vec{q} = \vec{k}_r - \vec{k}_i$) is given by

$$\left|\vec{q}\right| = 2\left|\vec{k}\right| \sin\frac{\theta}{2} = \frac{4\pi}{\lambda}\sin\frac{2\theta}{2}$$

Where 2θ is the scattering angle, i.e. the angle between the incident and the reflected wave vectors.

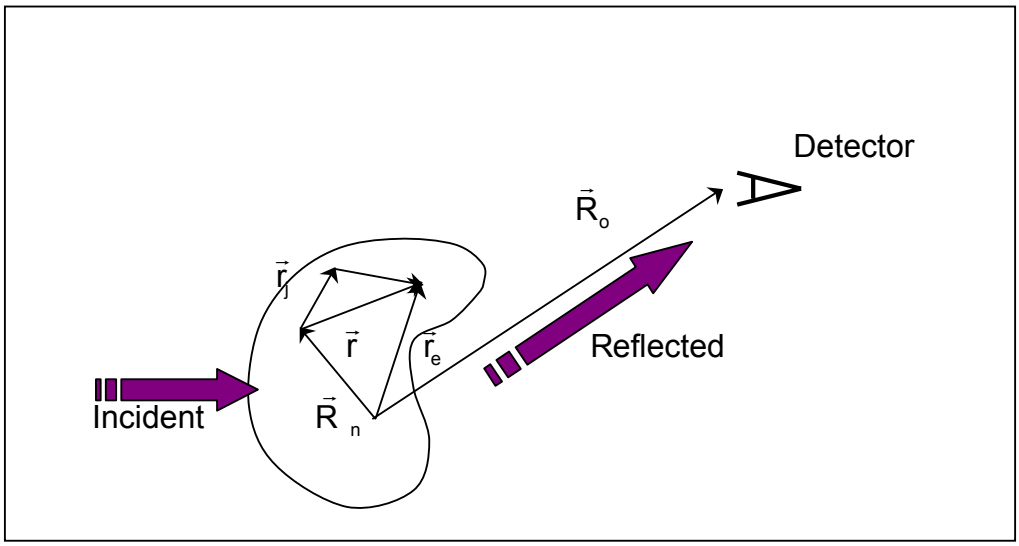

Figure 1-5 Schematics of x-ray diffraction

Using the concept of the momentum transfer vector, the amplitude of the incident and the reflected wave can be related by

$$A_r = A_i \frac{e^2}{mc^2}\frac{1}{R_o}\mathbf{exp(}i\vec{q}\cdot\vec{r}\mathbf{)}$$

Due to the small scattering cross-section of electrons it is safe to assume that the probability of the x-ray being scattered more than once before reaching the detector is infinitesimally small and the kinematical approximation holds true. Under the kinematical approximation the effect of a collection of electrons can be obtained by a linear sum of the effects of individual electrons. The atoms of the crystal can be represented by the density distribution of the electrons within them and the scattering can be modeled as an integral of this density distribution function over the volume of the atom.

$$A_r = A_i \frac{e^2}{mc^2}\frac{1}{R_o}\int_{-\infty}^{+\infty}\rho(\vec{r}')\,\mathbf{exp(}i\vec{q}\cdot(\vec{R}_n+\vec{r}_j+\vec{r}')\mathbf{)}d^3\vec{r}'$$

$$A_r = A_i \frac{e^2}{mc^2}\frac{1}{R_o}f(\vec{q})\,\mathbf{exp(}i\vec{q}\cdot(\vec{R}_n+\vec{r}_j)\mathbf{)}$$

Where $\vec{R}_n + \vec{r}_j$ is the position of the atom, and $f(\vec{q})$ is the atomic form factor. The atomic form factor is closely related to the density distribution of the electron in the atom in fact it is the Fourier transform of the density distribution function. Having obtained the scattering of x-rays by each atom the scattering of the unit cell of the crystal can be modeled by summing up the contribution from each atom of the unit cell and is given by the expression

$$A_r = A_i \frac{e^2}{mc^2} \frac{1}{R_o} \sum_{j=1}^{N} f_j(\vec{q}) \exp(i\vec{q} \cdot (\vec{R}_n + \vec{r}_j))$$

$$A_r = A_i \frac{e^2}{mc^2} \frac{1}{R_o} F(\vec{q}) \exp(i\vec{q} \cdot \vec{R}_n)$$

$$\text{where } F(\vec{q}) = \sum_{j=1}^{N} f_j(\vec{q}) \exp(i\vec{q} \cdot \vec{r}_j)$$

Atoms at different locations within the unit cell may not be the same therefore it is very important to distinguish them by separate form factors. $F(\vec{q})$ is called the structure factor of the unit cell and represents the effect of the entire unit cell on the incident x-ray.

Continuing on a similar argument the effect of the entire crystal can be obtained by summing the effects of individual unit cells. Due to the periodic nature of the crystal this yields sharply focussed patterns, which depends on the energy of the incident radiation and the angle of diffraction. These patterns are known as the diffraction pattern of the crystal. The position of each unit cell can be represented as:

$$\vec{R}_n = n_1\vec{a}_1 + n_2\vec{a}_2 + n_3\vec{a}_3$$

And the reflected wave is:

$$A_r = A_i \frac{e^2}{mc^2} \frac{1}{R_o} F(\vec{q}) \sum_{n_1=0}^{N_1-1} \sum_{n_2=0}^{N_2-1} \sum_{n_3=0}^{N_3-1} \exp(i\vec{q} \cdot (n_1\vec{a}_1 + n_2\vec{a}_2 + n_3\vec{a}_3))$$

$$A_r = A_i \frac{e^2}{mc^2} \frac{1}{R_o} F(\vec{q}) \sum_{n_1=0}^{N_1-1} \exp(in_1\vec{q} \cdot \vec{a}_1) \sum_{n_2=0}^{N_2-1} \exp(in_2\vec{q} \cdot \vec{a}_2) \sum_{n_3=0}^{N_3-1} \exp(in_3\vec{q} \cdot \vec{a}_3)$$

The summation over the entire crystal is simply a summation of a geometric series and the physics behind this effect has been taken care of by the structure

factor ($F(\vec{q})$). This particular geometric sum is called the slit function and is given by:

$$S_N(x) = \frac{1 - \exp(iNx)}{1 - \exp(ix)}$$

In real experiments the amplitude of the incident and reflected waves are imaginary and cannot be measured. The measured quantity is the intensity and is given by:

$I(\vec{q}) = A(\vec{q})\, A^*(\vec{q})$.

The intensity can also be expressed as:

$$\left|S_N(x)\right|^2 = \frac{\sin^2(Nx)}{\sin^2(x)}$$

Figure 1-2 shows the dependence of the N-slit function on the variable N, in our case the number of layers in the crystal.

The amplitude of the diffracted wave from the crystal can be expressed in terms of the slit function as

$$A_r = A_i \frac{e^2}{mc^2} \frac{1}{R_o} F(\vec{q})\, S_{N_1}(\vec{q}\cdot\vec{a}_1) S_{N_2}(\vec{q}\cdot\vec{a}_2) S_{N_3}(\vec{q}\cdot\vec{a}_3)$$

As can be seen in figure 1-6 the N-slit function approaches the delta function as N becomes very large, which is a reasonable assumption for crystals. For all values of N, the slit function has maxima at $X = 2N\pi, N = 0, 1, 2, ...$, thus the condition for maximum intensity (or maximum amplitude), in case or crystals is

$\vec{q}\cdot\vec{a}_1 = 2\pi h$

$\vec{q}\cdot\vec{a}_2 = 2\pi k$

$\vec{q}\cdot\vec{a}_3 = 2\pi l$

where $h, k, l \in \{0,1,2,.....\}$

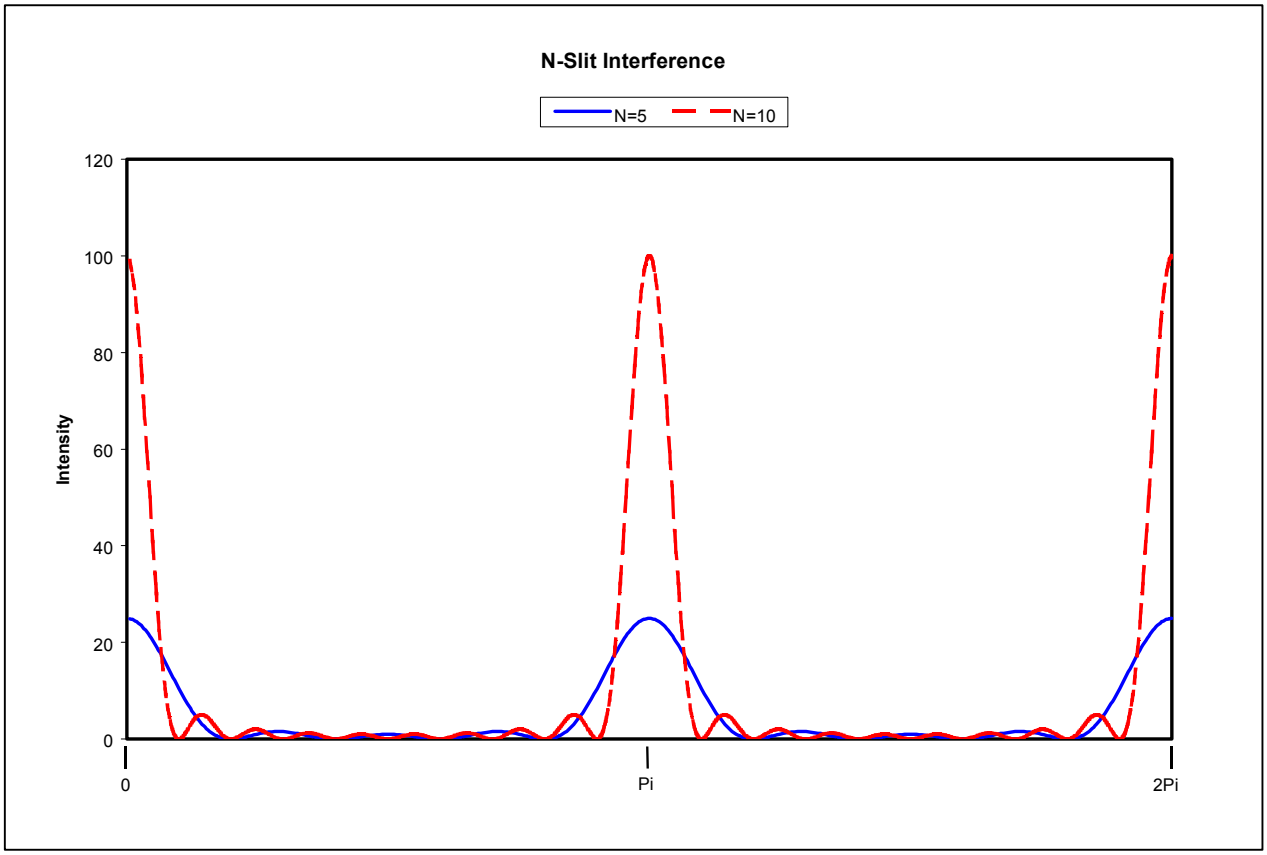

Figure 1-6 N slit interference function

These conditions, which must be met to have a strong reflection are called Lau condition (von Laue 1936) and h, k, l are called the Miller indices. The condition for maxima can be satisfied if:

$$\vec{q} = h\vec{b}_1 + k\vec{b}_2 + l\vec{b}_3$$

where

$$\vec{b}_1 = 2\pi \frac{\vec{a}_2 x \vec{a}_3}{\vec{a}_1 \cdot \vec{a}_2 x \vec{a}_3}$$

$$\vec{b}_2 = 2\pi \frac{\vec{a}_3 x \vec{a}_1}{\vec{a}_2 \cdot \vec{a}_3 x \vec{a}_1}$$

$$\vec{b}_3 = 2\pi \frac{\vec{a}_1 x \vec{a}_2}{\vec{a}_3 \cdot \vec{a}_1 x \vec{a}_2}$$

The three vectors $\vec{b}_1, \vec{b}_2, \text{and} \vec{b}_3$, by construction, span a vector space whose dimension is the same as the vector space spanned by $\vec{a}_1, \vec{a}_2, \text{and} \vec{a}_3$ and are

called the reciprocal lattice vectors. The points on the reciprocal lattice where the intensity is maximum (i.e. Lau conditions are satisfied are called the Bragg peaks)

1.4 Surface diffraction

Till this point we have discussed x-ray diffraction in a very general fashion. Existing methods using x-ray diffraction to determine crystal structures suggest that, similar methodology can be found to determine surface structures. In x-ray scattering the intensity of reflection in the reciprocal lattice can be expressed as a product of the atomic form factor and a simple geometrical structure factor. This simplicity that occurs because of the weak interaction between the x-rays and matter, i.e. each photon is backscatterred after a single encounter with a lattice ion. Another consequence of this kinematical scattering is that the spot intensities are independent of the incident beam energy and azimuthal angle of incidence. This simplicity makes x-ray a very suitable probe for determining surface structures.

Consider the ideal monolayer of atoms as shown in figure 1-7. The diffraction pattern of such a structure can be obtained by putting $N_3 = 1$ in the expression for the amplitude of diffracted wave giving

$$A_r = A_i \frac{e^2}{mc^2}\frac{1}{R_o}F(\vec{q})\, S_{N_1}(\vec{q}\cdot\vec{a}_1)S_{N_2}(\vec{q}\cdot\vec{a}_2)S_1(\vec{q}\cdot\vec{a}_3) \Rightarrow$$

$$A_r = A_i \frac{e^2}{mc^2}\frac{1}{R_o}F(\vec{q})\, S_{N_1}(2\pi h)S_{N_2}(2\pi k)$$

The diffraction pattern is sharp in the h and k direction but completely diffuse in the l direction and can be viewed as a diffuse (only in the l direction) rod and not as a point as shown in figure 1-8(a).

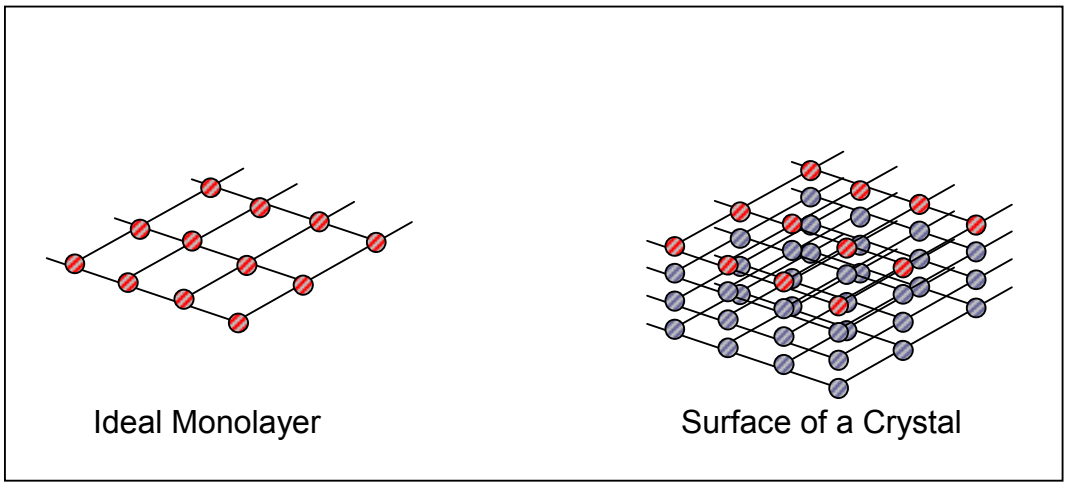

Figure 1-7 Possible 2D structures

However it is impossible to create an ideal monolayer and in real life the surfaces to be studied are always associated with a bulk. Figure 1-8(b) shows the diffraction pattern of a surface superimposed with the bulk. In the figure the contribution to the intensity, of the diffracted wave, from the surface and the bulk have been added. This is not a realistic picture due to the coherent nature of the incident wave it is not the intensities but rather the amplitudes which should be added. The picture is merely to convey the idea that the diffraction rods of the surface pass through the diffraction peaks (Bragg peaks) of the bulk. The real intensity profile can be understood by considering the behavior of the Slit function.

If the number of layers is large, then the term representing the numerator of the Slit function varies rapidly and the experimentally measured quantity is the average intensity of the numerator due to the finite resolution of the apparatus (average of a sinusoidal function is ½). Thus the small variation in the Slit function, due to the rapidly changing numerator can be smeared out.

$$\left|S(\vec{q}\cdot\vec{a}_3)\right|^2 = \frac{1}{2\sin^2(\vec{q}\cdot\vec{a}_3/2)}$$

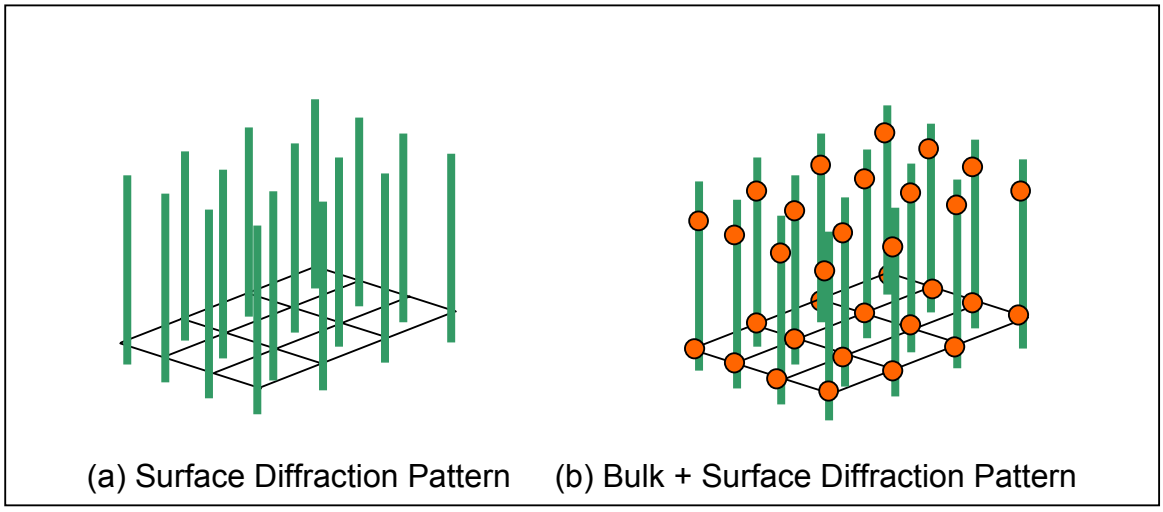

Figure 1-8 Diffraction Pattern from ideal monolayer and surface

This expression gives the value of the intensity along the rod except for the near neighborhood of the Bragg peaks. This simplification is not valid near the Bragg peak ($\vec{q}\cdot\vec{a}_3 = 2\pi l$). Near the Bragg peak the variation of the numerator in the Slit function is large and the value cannot be replaced by the average. Such a rod whose intensity is given by the equation is called a Crystal Truncation Rod (CTR). The intensity variation along a rod can also be explained by considering the contributions from all the layers of a semi-infinite crystal.

$$S(\vec{q}\cdot\vec{a}_3) = \sum_{j=0}^{\infty} \mathbf{exp}(-i\vec{q}\cdot\vec{a}_3 - \varepsilon)j$$

$$= \frac{1}{1-\mathbf{exp}(-i\vec{q}\cdot\vec{a}_3 - \varepsilon)}$$

The quantity ε represents the attenuation of the incident wave from one layer to the next inside the crystal. As the attenuation approaches 0 the Amplitude Square of $S(\vec{q}\cdot\vec{a}_3)$ approaches the previous expression.

The intensity of the CTRs not only on the momentum transfer vector but also roughness. The surface of a semi-infinite crystal can be modeled using step function. The diffraction pattern (Fourier transform of the density function) is the convolution of the reciprocal lattice with $(i\vec{q}\cdot\vec{a}_3)^{-1}$. A simple model of roughness (Robinson 1986) is the exponentially decaying function, where the number of

atoms falls off exponentially from one layer to the next. The expression for the intensity of a rough surface is given by:

$$I_{rough} = I_{CTR}\frac{(1-\beta)^2}{1+\beta^2-2\beta\cos(\vec{q}\cdot\vec{a}_3)}$$

Where β is the roughness model parameter.

As shown before the diffraction pattern and the density function are Fourier transforms of each other related by:

$$F(\vec{q}) = F_{hkl} = \int \rho(\vec{r})\exp(i\vec{r}\cdot(h\vec{b}_1 + k\vec{b}_2 + l\vec{b}_3))d^3\vec{r}$$

or

$$\rho(\vec{r} = \int F(\vec{q})\exp(-i\vec{r}\cdot\vec{q})d^3\vec{q}$$

At a first glance determining the structure ($\rho(\vec{r})$) from the diffraction pattern might appear as a simple integration, however the problem arises from the fact that in general F_{hkl} is a complex quantity and can be represented by an amplitude and a phase $F_{hkl} = |F_{hkl}|e^{i\alpha_{hkl}}$. The experimentally measured quantity is the amplitude of the structure factor and the information about the phase is lost. Information about the lost phase can be retrieved using some powerful techniques. Use of Patterson function is one such technique.

Patterson function for a diffraction patters is defined as:

$$P(\vec{r}) = \sum_{h,k,l}|F^2{}_{hkl}|\exp(-i\vec{q}\cdot\vec{r})$$
$$= \int \rho(\vec{r}+\vec{R})\rho(\vec{R})d^3\vec{R}$$

The Patterson function, as expressed above, is the auto-correlation function of the density function and can be evaluated from the experimental data since the information about the phase is not required. It is apparent that all the interatomic distances of the unit cell will be present in the Patterson function thus a peak in the Patterson function represent an interatomic distance. Figure 1-9 shows the density function and the corresponding Patterson function for a one-dimensional unit cell. Patterson functions provide crystallographers with a very useful technique of solving the problem of the lost phase however for very large structures this method can seem confusing and difficult to approach.

Interference of the bulk and the surface is another useful technique that is used to estimate the structure of the surface from the data. This method however needs an initial guess of the structure. The initial guess is common to every fitting technique since the convergence of the fit to the right solution may depend on the starting point. The model (also known as the fitting) model is allowed to adapt towards the data by making the position of the atoms within the model parameterized. The structure factor of the model can be calculated as a function of these parameters. A measure of agreement between the data and the calculated structure factor is the χ^2, given by:

$$\chi^2 = \frac{1}{N-P}\sum \frac{\left(\left|F_{Calc}(h,k,l)\right| - \left|F_{Obs}(h,k,l)\right|\right)^2}{\sigma^2_F}$$

Where N is the total number of data point, P is the total number of fitting parameters and σ_F is the standard deviation of the data. Given a sufficient number of data points and a good starting point this method s capable of determining the structure of the surface very accurately.

1.5 Debye-Waller Factor

Effects of thermal vibrations have not been considered, in our analysis of x-ray diffraction of solids and surface, till this point. Previous expressions for the intensity of the diffraction pattern, at a given point in the reciprocal space, were derived assuming that the atoms occupy definite positions in crystal. The model for the probability distribution function of the atoms was simply a delta function. This model is appropriate enough to introduce the concepts of diffraction and explanation of Bragg peaks, however when it comes to fitting experimental data it is very crucial to account for the thermal vibrations of the atoms within the crystal. In the classical model for solids the atoms interacts with its neighbors by electromagnetic interaction. The equilibrium position of the atom (the lattice site) is the position where the interatomic potential energy is minimized. Thus the atom can be viewed as an oscillator with the minimum of the potential energy at the lattice site. The quantum mechanical model of solids uses the same principle with the exception that the position of the atom, within the interatomic potential, is

expressed in terms of it's density distribution function, also known as the probability distribution function (P.D.F) of the wave function.

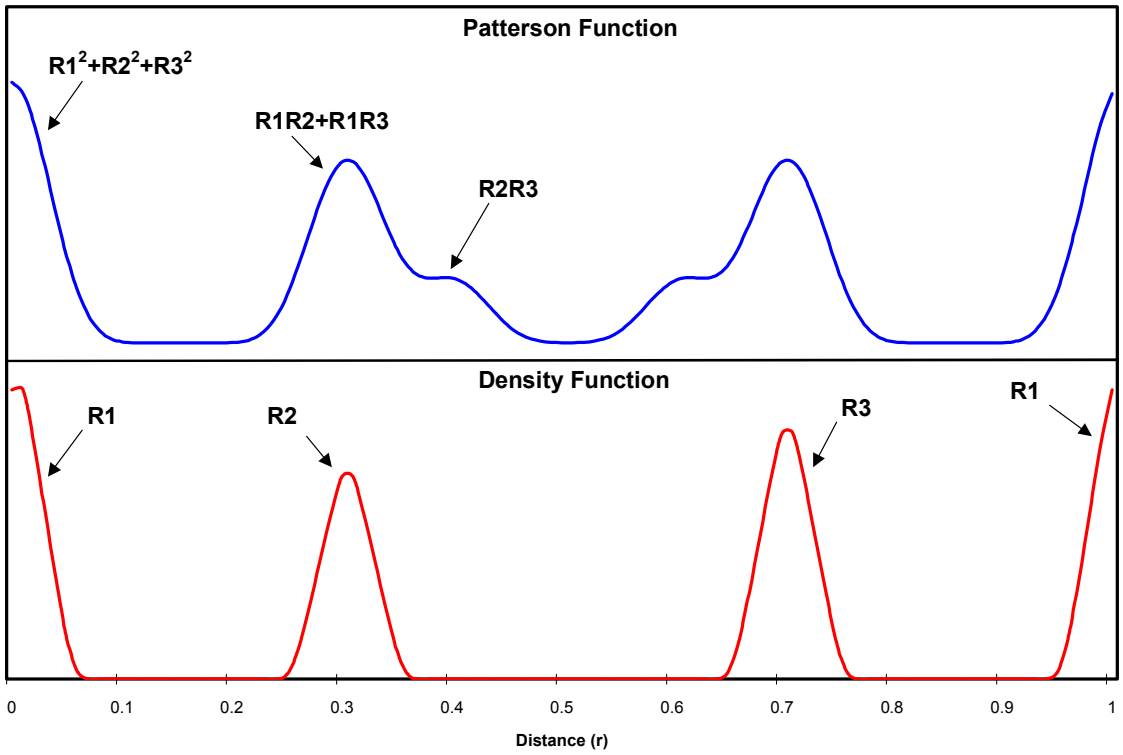

Figure 1-9 Density function and Patterson function of a simple one dimensional model. The periodicity of the structure is 1 normalized units

In general the density function of the atom depends on the nature of the interatomic potential. To keep things simple only the harmonic interatomic potential will be considered (anharmonic effects are discussed in later chapters) and only the ground state of the atom in the interatomic potential will be considered. The excited states do not play a significant role, except at high temperatures.

The density function of the electron within the atom can be related to the thermal vibrations as

$$\rho'(\vec{r}) = \int_{-\infty}^{+\infty} P(\vec{u})\rho(\vec{r}-\vec{u})d^3\vec{u}$$

Where $\rho(\vec{r})$ is the density distribution function of the electron within the atom, $P(\vec{u})$ is the density distribution function (Probability Distribution Function P.D.F)

of the atom within the interatomic potential well. The overall density distribution function of the electron, as a result of the thermal vibrations, is a convolution of the density distribution of the electron within a stationary atom and the density distribution function of the atom itself.

Thus the atomic form factor due to the thermal vibrations can be expressed as:

$$f'(\vec{q}) = \int_{-\infty}^{+\infty} \rho'(\vec{r}) e^{-i(\vec{q}\cdot\vec{r})} d^3\vec{r}$$

$$= \int_{-\infty-\infty}^{+\infty+\infty} P(\vec{u})\rho(\vec{r}') e^{-i\vec{q}\cdot(\vec{r}'+\vec{u})}\, d^3\vec{r}' d^3\vec{u}$$

where the position of the electron has been expressed as vector sum of the position of the atom and the position of the electron within the atom

$$\vec{r} = \vec{r}' + \vec{u}$$

Since the two variables $\vec{r}'$ and $\vec{u}$ are independent the atomic form factor can be expressed as:

$$f'(\vec{q}) = \int_{-\infty}^{+\infty} \rho(\vec{r}') e^{-i\vec{q}\cdot\vec{r}'} d^3\vec{r}' \int_{-\infty}^{+\infty} P(\vec{u}) e^{-i\vec{q}\cdot\vec{u}} d^3\vec{u}$$

$$= f(\vec{q})T(\vec{q})$$

Where $T(\vec{q})$ is the Fourier transform of the density distribution function of the atom within the interatomic potential.

As mentioned before, for the sake of simplicity the interatomic potential is assumed to be harmonic (anharmonic effects will be introduced in later chapters). The P.D.F. of the atoms in a harmonic potential is Gaussian

$$P(\vec{r}) = \frac{\alpha}{\sqrt{\pi}} e^{-\alpha^2|\vec{r}|^2}$$

As seen before the Fourier transform of the convolution integral in the real space is the product of the two Fourier transforms

$$f'(\vec{q}) = \int_{-\infty}^{+\infty} P(\vec{u}) e^{-i\vec{q}\cdot\vec{u}} d^3\vec{u} \int_{-\infty}^{+\infty} \rho(\vec{r}') e^{-i\vec{q}\cdot\vec{r}'} d^3\vec{r}'$$

$$= f(\vec{q}) \int_{-\infty}^{+\infty} \frac{\alpha}{\sqrt{\pi}} e^{-\alpha^2|\vec{u}|^2} e^{-i\vec{q}\cdot\vec{u}} d^3\vec{u}$$

=

The integral can be expressed as the expectation value of the function $e^{-i\vec{q}\cdot\vec{r}}$

$$f'(\vec{q}) = f(\vec{q})\left\langle e^{-i\vec{q}\cdot\vec{u}}\right\rangle = f(\vec{q})\left[1 + i\left\langle|\vec{q}\cdot\vec{u}|\right\rangle - \tfrac{1}{2}\left\langle|\vec{q}\cdot\vec{u}|^2\right\rangle - \tfrac{1}{6}i\left\langle|\vec{q}\cdot\vec{u}|^3\right\rangle .....\right]$$

For a Gaussian P.D.F the terms with odd powers vanish since the P.D.F is an even valued function. It can be shown that for a Gaussian P.D.F.

$$\left\langle e^{ikx}\right\rangle = e^{-1/2k^2\left\langle x^2\right\rangle}$$

Thus the modified atomic form factor is given by

$$f'(\vec{q}) = f(\vec{q})\,\mathbf{exp}\left(-\tfrac{1}{2}\left\langle|\vec{q}\cdot\vec{u}|^2\right\rangle\right) = f(\vec{q})e^{-M}$$

The observed intensity is modified by the same factor

$$I'(\vec{q}) = |f(\vec{q})|^2 = I(\vec{q})e^{-2M}$$

This is the well-known Debye Waller factor (Debye 1913, Waller 1923). The above equation is not exact if the P.D.F. is not Gaussian but for small values of $\left\langle\vec{u}^2\right\rangle$ this is still a good approximation.

The Debye-Waller factor is proportional to the magnitude of the momentum transfer vector ($|\vec{q}|^2 = \frac{16\pi^2}{\lambda^2}\mathbf{sin}^2\frac{2\theta}{2}$), thus the effects of thermal vibration are more pronounced for smaller wavelengths and larger scattering angle.

1.6 Surface Reconstruction

Cleavage of a crystal, to produce a surface destroys the translational symmetry of lattice in the direction normal to the surface. At first one might think that this does not perturb the rest of the material much, i.e. the arrangement of the atoms on the surface is the same as a planar termination of the bulk. This so-called ideal surface is rather an exception than a rule. However as any other exception they do occur once in a while. A classic example of such a crystal is the rocksalt. Rocksalt is an ionic crystal and the cubic structure of the bulk arises because this particular arrangement of ions leads to minimization of electrostatic energy. Consider any two planes within this crystal that are parallel to the intended cleavage surface. Since both these planes are neutral there is only a

very weak Coulomb interaction between them. Hence, the creation of the surface has almost no effect on the ion position of the exposed surface.

In metals, the Wigner-Seitz charge cloud formed by the conduction electrons screens the ionic core. Due to this screening effect the residual interactive forces between the ionic cores are weakly attractive and stabilize the closed packed structure of the bulk when Pauli ‘s exclusion is included. At the surface of the metal the electrons are free to redistribute themselves to lower the energy. This redistribution of electrons at the surface results in smoothing of the surface electronic charge as shown in figure 1-10. The smoothing of the surface charge leaves the ions out of electrostatic equilibrium with a new asymmetric screening distribution. The net effect of this new distribution is a contractive relaxation due to the unbalanced forces.

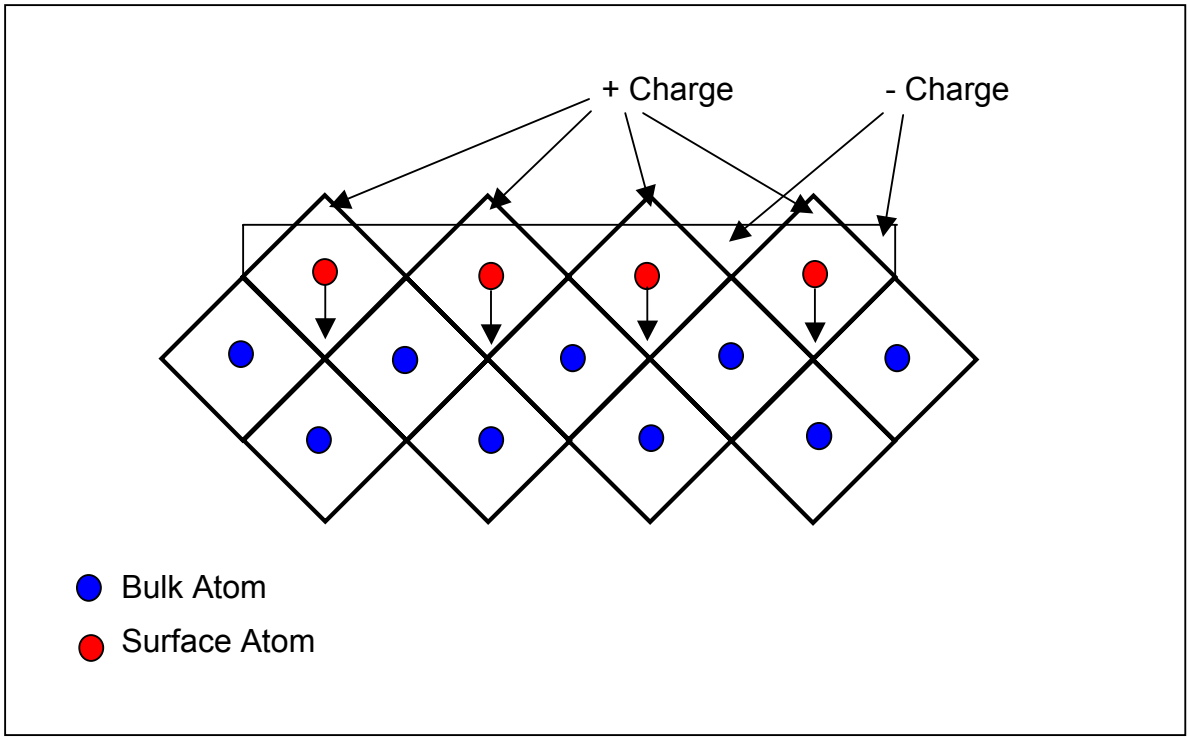

Figure 1-10 Contraction of surface in metals

Such a reconstruction of surface leading to a contraction is seen in may metals like Cu(111), Pt(111) etc. The dynamics at the surface for semiconductors is entirely different. The directional chemical bonds between atoms favor the tetrahedral coordination as seen in diamond and Si (figure 1-3). A highly unstable

state occurs when these bonds are broken at the surface. The surface and subsurafec atoms pay considerable elastic distortive enegryin order to reach a structure that facilitates new bon formation. Beyond this there are very few general predictive principles and the resulting reconstruction of the surface, for semiconductors, yields geometrical structures that are much more complex than the ideal surface termination.

In some cases the reconstruction may involve relaxation of the atoms in the out of plane direction e.g. $NiSi_2$, without changing the lattice constant in the in-plane direction. It is also possible that the reconstruction may involve relaxation of in-plane and out of plane relaxation changing the size of the unit cell drastically, e.g. the 7x7 reconstruction of the Si(111) surface. The term 7x7 reflects that the unit cell of the reconstructed surface is 7 times large than the unit cell of the unreconstructed surface in the in-plane direction. Thus the unit cell of the Si(111)7x7 surface contains 49 (7^2) unit cells of the bulk. Such large reconstruction is typical of covalent materials where the elastic strain of the surface is long range.

Crystal structures of bulk can be theoretically calculated by energy minimization methods. The translational invariance restricts the number of ion positions that can be independently varied in any computational energy minimization scheme. The problem is much more difficult at the surface since the translational symmetry is destroyed at the bulk, in the direction normal to the surface. This makes it very difficult to theoretically determine surface crystal structures.

At the surface the translational symmetry of the bulk is destroyed in the direction normal to the surface. One still retains the translational symmetry in the in-plane direction. For a strictly tow dimensional periodic structure every lattice point can be reached from the origin by a translation

$$\vec{R} = n_1\vec{a}_1 + n_2\vec{a}_2$$

Where $\vec{a}_1$ and $\vec{a}_2$ define a coordinate system or mesh for the surface. There are five such possible mesh as shown in figure 1-11. The specification of an ordered surface structure requires both the unit mesh and the location of the basis atom

at each point of the mesh. The position of the atoms must be consistent with the symmetry operation (symmetry group) of the surface struture. In two dimension the only possible operations, that leave one point unmoved are:

1. **Reflection:** A mirror operation across a line
2. **Rotation:** Rotation through $2\pi/p$ where p = 1, 2, 3, 4, and 6

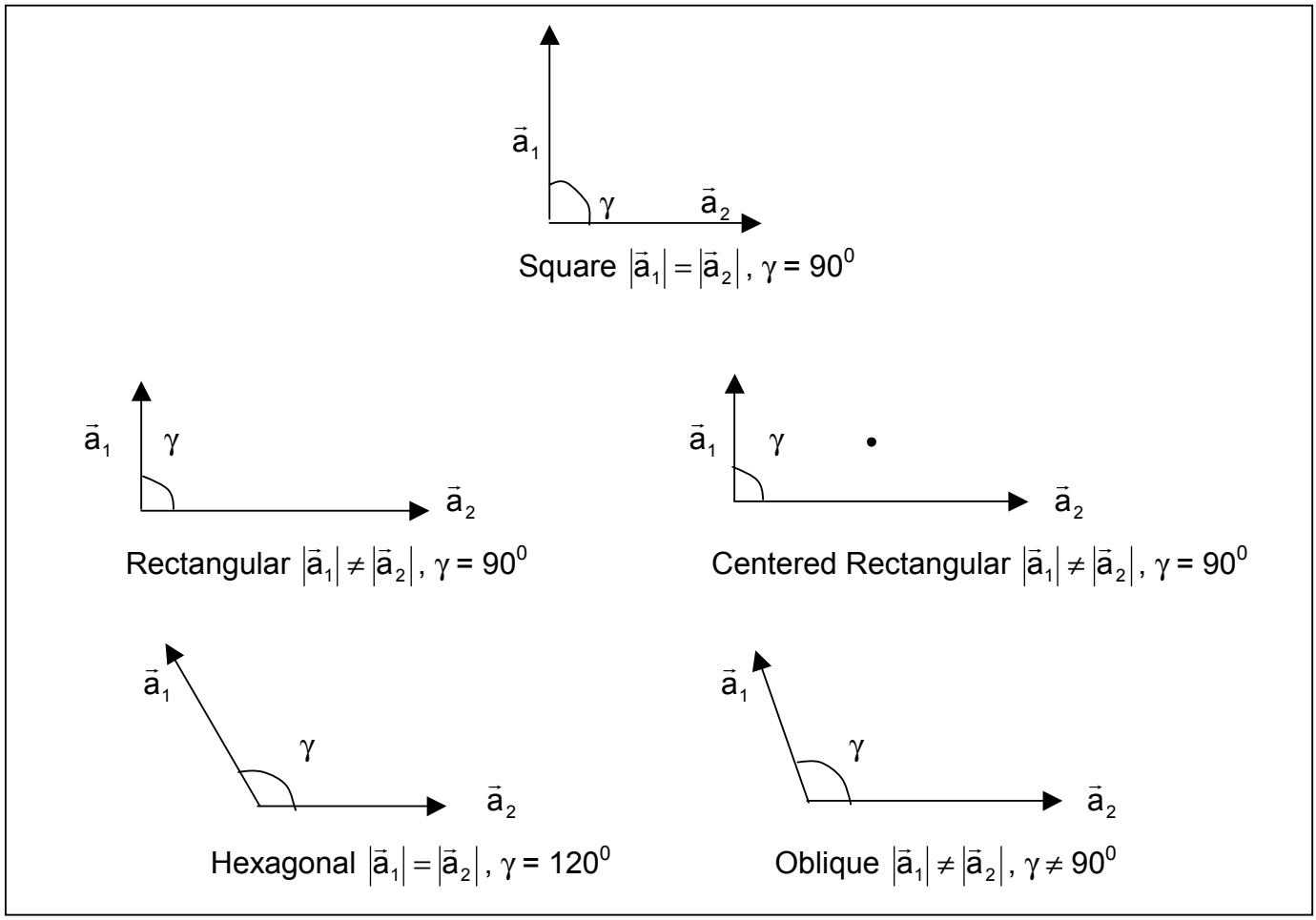

Figure 1-11 Surface coordinate systems

As mentioned earlier the semi-infinite model of the crystal is a fairly accurate one, since the number of atoms as seen by the probe in the in-plane direction is very large. In the out of plane direction the diffraction pattern can be modeled using Crystal Truncation Rods and the roughness function. One of the most widely studied reconstruction is the 7x7 reconstruction of Si(111). A detailed

model for this structure was first proposed by Takayanagi et. al. (1986). Details of this reconstruction will be provided in chapter 2. This study is geared towards understanding the detail three dimensional structure of the 7x7 reconstruction of Si(111) and its phase transition at high temperatures.

1.7 Synchrotron X-ray diffraction

X-ray scattering has been one of the most successful technique in determining structural properties of surfaces and understanding physics of 2D systems. The scattering cross-section of X-rays are very well understood, and to a large degree independent of the chemical environment, which makes X-ray a very reliable probe for structural analysis. For X-rays to be used in structural analysis of 2D systems two problems must be overcome. Firstly a sufficiently bright source of radiation is required since the scattered signal from the surface is much weaker than the signal scattered from the bulk. This problem was overcome with the advent of synchrotron radiation sources. Secondly it is important to separate the contribution from the bulk and surface which can be achieved by:

I. By studying reflection from the surface which are crystallographically distinguishable from bulk reflections (e.g. supper-lattice reflections from reconstructed surface).
II. By using total internal reflection to limit the penetration of X-ray into the bulk.

1.7.1 Basic Scattering Geometry

The essential technique in high resolution scattering is the precise orientation of the sample in the incident X-ray beam and of the analyzer with respect to it. The conventional 4-circle diffractometer achieves this by defining a “scattering plane” containing the incident and the scattered beam. The analyzer moves only in this plane defined by the 2θ angle. The sample rotates in three Eularian axes (θ, ϕ, and χ). Any position of any reflection in the reciprocal space can be

mapped on to the 4 angles with help of the wave vector ($k=1/\lambda$). Since the number of unknown quantities (4) is larger than the minimum number required to define a position in the reciprocal space (3) there is a certain amount of redundancy in the mapping. This redundancy allows one additional geometric constraint to be imposed; the grazing angle of incidence is an example of such a constraints. The grazing angle prevents the penetration of the X-ray into the bulk to a large degree. Figure 1-12 shows the complete view of the diffratometer viewed towards the X-ray source. The significant difference between this instrument and previous designs is the direct coupling of the sample motion into a stationary vacuum chamber is accomplished with a differentially pumped teflon sealed feedthrough and a welded bellows. This arrangement allows:

I. Uncompromised X-ray position
II. Standard state of the art surface preparation tools
III. Operation of the instrument as a 4-circle diffractometrer
IV. Flexible chamber arrangement that can easily incorporate future modifications

The system has two modes of operation. First, during X-ray scattering experiments the sample is moved to the extreme right, pulling the sample against a pedestal. This pedestal ensures proper allignement of the sample in the X-ray beam, and allows for free but limited rotation of the sample with the 4-circle diffractometer. In the second mode which allows the sample to be accessed by a full range of surface probes, the manipulator is extended into main vacuum chamber by contraction of the long bellow.

The X-ray diffractometer is based on the standard Huber 430/440 diffractometer combination. The χ circle of the standard Huber 5020 4-circle diffractometer by a pair of 5020 arc due to the space limitation. A Huber 421 was used instead of the 410 for the φ circle to increase the bore size and increase the torque provided.

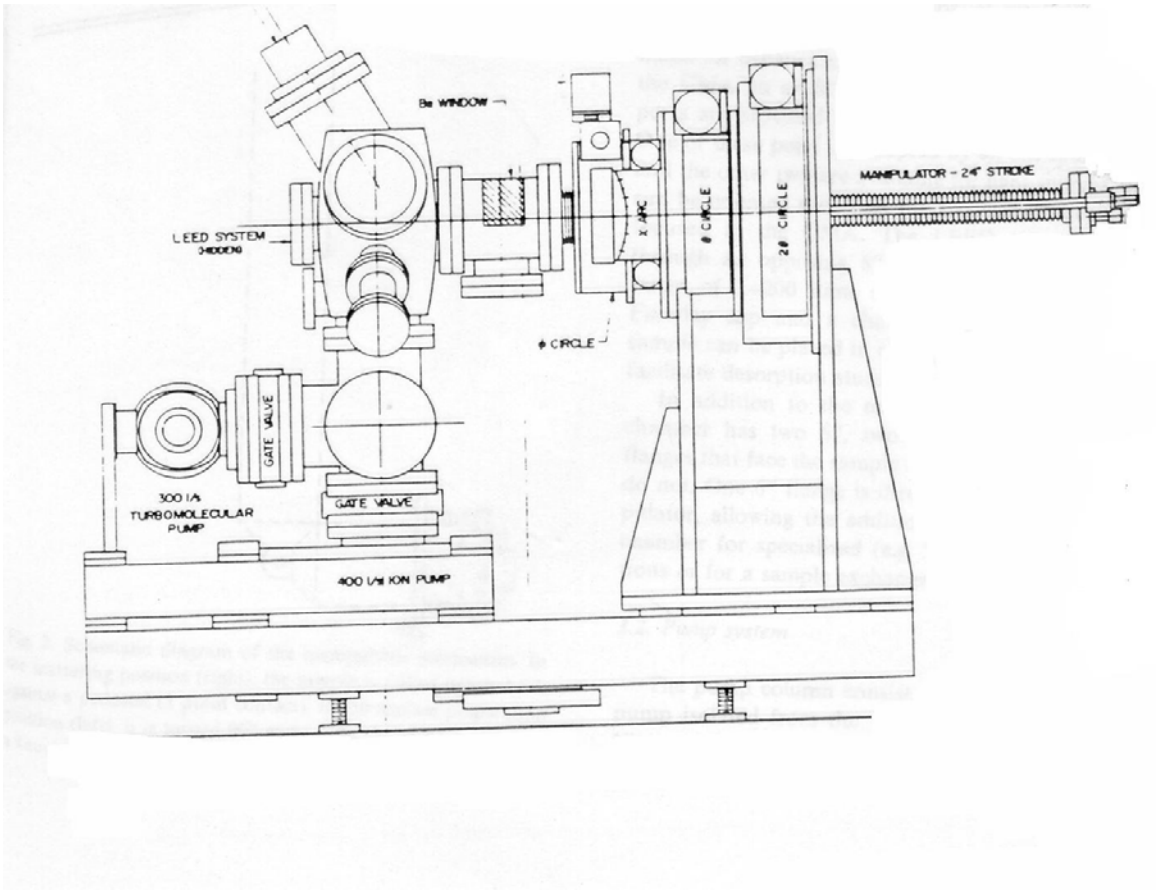

Figure 12 4-Circle Huber Diffractometer

2. Structure of Si(111)7x7 Reconstruction

2.1. Introduction

Understanding the structure of a crystalline solid is a very crucial information. It is through this understanding that we can explain or predict it's other properties e.g. elasticity, band structure, magnetic property etc. This holds more so for surfaces since the structure and properties of a material can be radically different at times at the surface than in the bulk. In recent years it has been seen that anharmonicity of inter-atomic potential can sometimes play a very important role in determining the structure of solids and at specially surfaces (Meyerheim et. al. 1996, Gustaffson et. al. 1994, 96).

Anharmonicity of interatomic potential and it's effect is a well studied subject for bulks. One of the most classic manifestations of anharmonicity is the thermal expansion of solids. Since the early works of Debye & Waller (Debye & Waller 1923) large amount of theoretical and experimental work has been performed in understanding the effect of thermal vibration on Bragg and diffuse scattering. In contrast to this surprisingly little work has been done to understand and observe the effects of anharmonicity on surface. Anharmonicity is more predominant at the surface, than at the bulk, since the nearest neighbors is asymmetric due to the truncation of the solid. In a recent (Meyerheim et. al. 1996) the importance of anharmonic thermal vibration on the x-ray diffraction pattern of the surface has been shown. The surface studied in this work was a Cs monolayer on the Cu(001) surface. It was shown using a Fourier difference analysis that anharmonicity of the thermal vibration is important in obtaining the correct structure factor. The difference Fourier analysis predicts the positive (negative) atomic densities that need to be added (subtracted) to the model to explain the observed diffraction pattern.

$$\Delta\rho(x, y) = \sum_{h,k} \left(F_{hk0}^{obs} - F_{hk0}^{calc}\right) \cos(2\pi(hx + ky))$$

The pronounced maxima and minima of the difference Fourier map in case of the Cs monolayer on Cu(001) indicates that the thermal vibration of of

atoms in some surfaces cannot be explained by harmonic interatomic potentials only and that one needs to include anharmonic terms.

In another recent study (Gustaffson et. al. 1994, 96) on metal surfaces (Cu(111) and Ag(111)) explains the anomalous thermal expansion of the surface, in the direction normal to the surface, by including the effects of anharmonicity. As explained in the previous chapter, metal surfaces are contracted due to unbalanced distribution of the electrons at the surfaces. This unbalanced distribution applies a net inward force on the surface atom causing the surface layer to contract in the normal direction. It was seen, using medium energy ion scattering that the contraction becomes more prominent as the temperature increases till an inversion temperature is reached after which the surface begins to expand with increasing temperature. The large expansion coefficient can be explained by the anharmonicity of the interatomic potential of the surface atoms. In this chapter we investigate the effects of anharmonicity of the Si7x7(111) surface on it's diffraction pattern.

2.2. Si 7x7

Si, being a covalent, is expected to have a very different nature of anharmonicity at the surface than metals, and it is shown in this study that the anharmonicity is responsible for breaking symmetry of the x-ray diffraction pattern of Si(111)7x7 reconstruction.

Si(111)7x7 is one of the most widely studied surface, due to its complexity in structure. The complexity of the structure arises from the fact that elastic strain is long range in covalent solids like C & Si. Strong bond length constraints make bond bending as the means of relieving elastic strain which makes the unit cell of the reconstructed Si(111) surface very large and complex. Si(111)7x7 surface has been studied by different groups using different techniques. It was shown by Bennet (Bennet et. al. 1983) that the Si7x7 surface consists of alternating domains of faulted and unfaulted stacking. In this study is was shown using ion channeling that the surface peak along the [111] direction is almost identical to that of the bulk, but in the [001] and [11-1] direction the surface shows additional

peaks. The additional peaks can be explained by the presence of stacking fault, which does not effect the structure when viewed from the [111] direction.

There were other studies resulting in understanding the various aspects of the Si7x7 structure, e.g. Binnings (Binnings et. al.) showed the presence of adatom on the surface.

The currently accepted model of the Si7x7 surface was presented by Takayanagi in 1986 and is known as the DAS (Dimer, Adatom, and Stacking Fault) model. The DAS model as shown in figure 2-1 consists of a triangular lattice of atoms connected to the bulk by alternating 'normal' and 'faulted stacking[4] sequences, and on the top is an array of 'adatoms' each satisfying three bonds that would otherwise dangle from the truncated surface. The DAS model however does not include the relaxation of atoms, the information for which can be found only by experimental studies by theoretical energy calculations. Several studies (Robinson et. al. 1988, Robinson et. al 1992, Brommer et. al. 1991, Stich et. al. 1991, 1994, Chadi et. al. 1986) have refined the DAS model using different experimental and theoretical techniques. A detailed 2D model of the surface was given by Robinson in 1992.

The DAS model assumes a p6mm symmetry of the reconstructed Si(111)7x7 surface which is different form that of the underlying bulk which is p3m1. The projection of the model onto the 2D plane agrees quite well with previous and current experimental works. Previous studies on this subject by STM[2], TED[1], and X-ray diffraction[3,9,5] have provided a fairly accurate 2-D (2 Dimensional) model of the Si7x7 reconstructed surface.

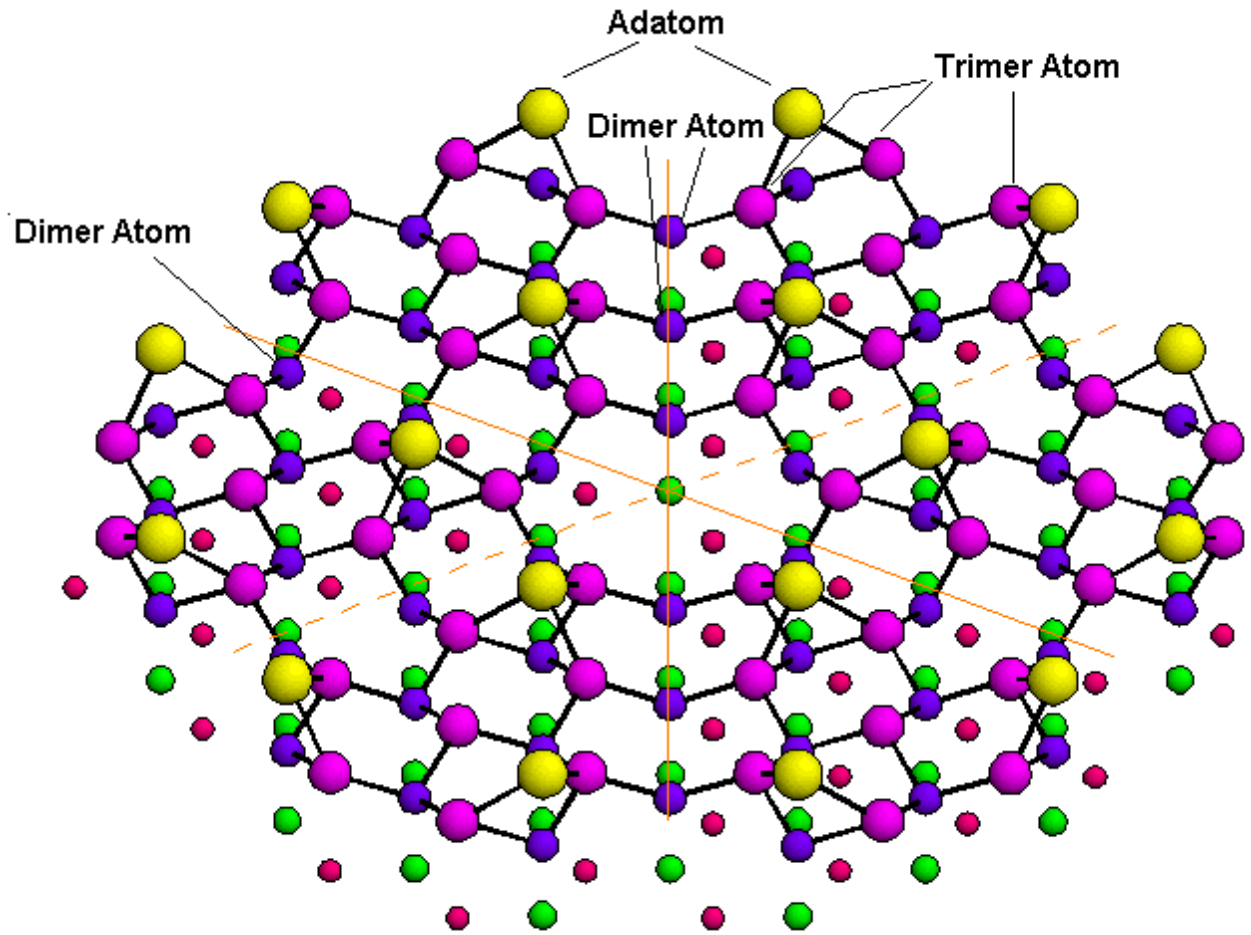

Figure 2-1 DAS model of Si7x7(111) reconstruction

Some experiment have shown that a lateral compression of the Ge(111) surface leads to a 7x7 reconstruction, indication a strong relationship between surface stress and reconstruction. This idea is also reinforced by the theory of epitaxy: by Frank and van de Merwe[**]. This theory relates to the strain energy of a thin crystalline layer connected to a bulk with different lattice spacing. When the crystalline layer is sufficiently thick, relieving the stress becomes energetically favorable. An unreconstructed Si(111), whose radial bond length is longer than the bulk, would be under a compressive stress since it is forced to have the same lattice spacing as the bulk underneath.

However not much effort has been made towards understanding the nature of the 3D structure. Most of the existing understanding of the 3D model comes from studies like x-ray reflection[5, 9] and RHEED[**]. While these studies are reliable they are not very conclusive because of the complexity of the structure. Some theoretical studies[11, 12] show that the adatoms are energetically favorable[8] since they lead to inward relaxation of the trimer of atoms below and hence is a means of relieving stress. Thus an unreconstructed Si(111) surface is strained and reconstruction is a way of relieving this stress. Reconstruction also helps in relieving the stress by introducing misfit dislocation, like the stacking fault, which gives rise to lines of dimers separating island with ‘normal’ and ‘faulted’ stacking. The stacking fault reduces the average number of atoms in a layer thus decreasing the stress.

The symmetry of the 7x7 surface (p6mm) being higher than that of the bulk (p3m1) is something to be considered carefully since this decreases the degrees of freedom for the surface atom to undergo relaxation. The 2D in plane ($q_{\perp} = 0$) experimental data agrees with the DAS model and indicates that the symmetry of the surface to be p6mm. It must be noted that the 2D data is sensitive not to the entire structure but rather to the projection of the structure onto the xy plane. It is quite possible for this projected structure to have a higher symmetry than the 3D structure thus the in plane data cannot distinguish

between the two symmetries. Theoretical studies by Stich[11, 12] et. al. show a slight breaking of the symmetry but this effect is very small and not conclusive.

The objective of this study is to understand the nature of the 3D structure of the reconstructed Si(111)7x7 surface. As mentioned earlier the symmetry of the DAS model is p6mm as opposed to p3m1 of the bulk Si. Figure 2-2 compares these two symmetries.

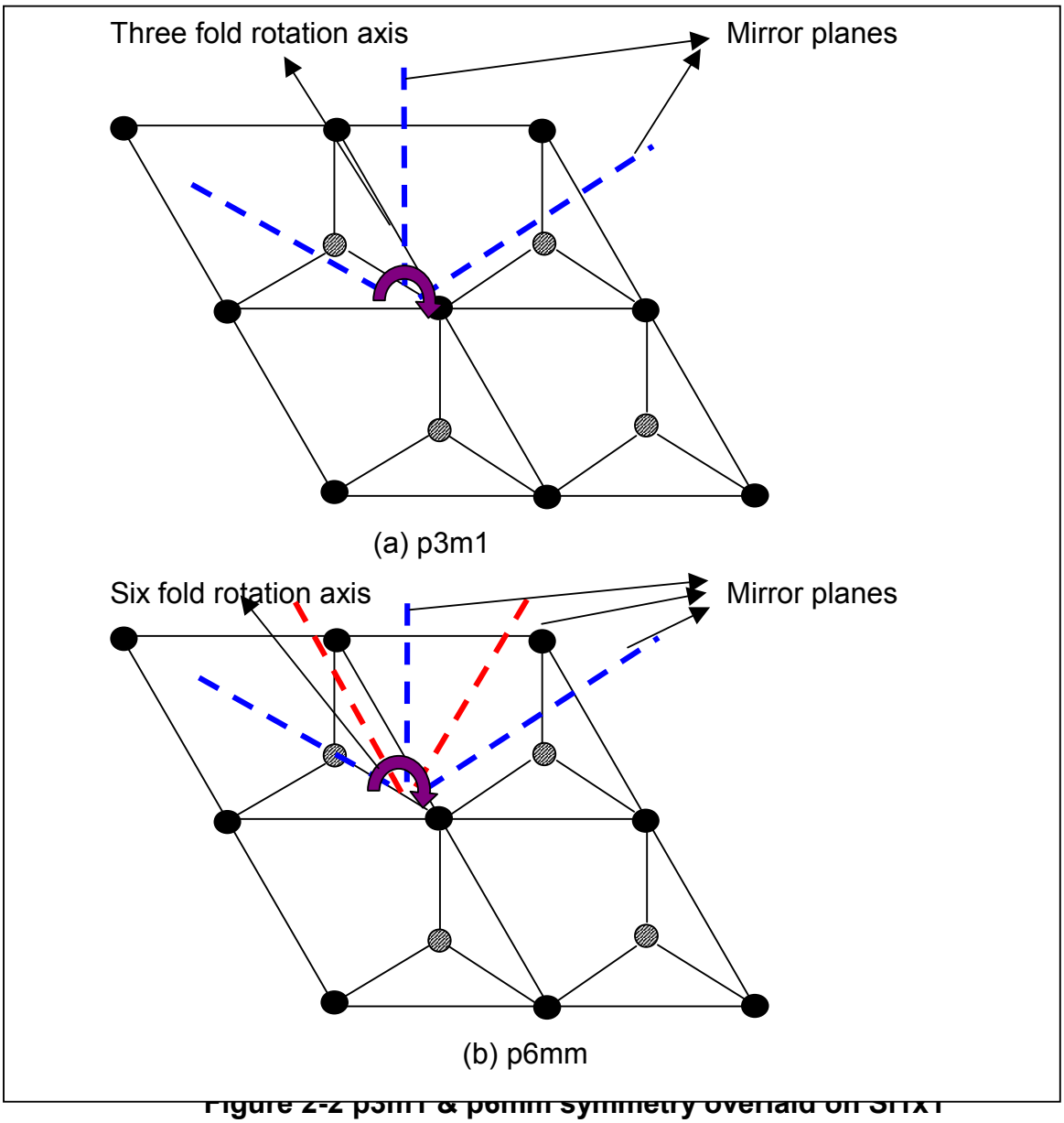

Figure 2-2 p3m1 & p6mm symmetry overlaid on Si1x1

From figure 2-2 it can be seen that the unit cell of the Si1x1 surface complies with the p3m1 symmetry but not p6mm symmetry. Due to the presence

of stacking fault in the Si7x7 unit cell additional mirror line (shown in red) are present. The diffraction pattern from a structure having p3m1 symmetry is expected to show a three fold symmetry about the center axis and a structure with p6mm symmetry is expected to show a 6 fold symmetry about origin, as shown in figure 2-3.

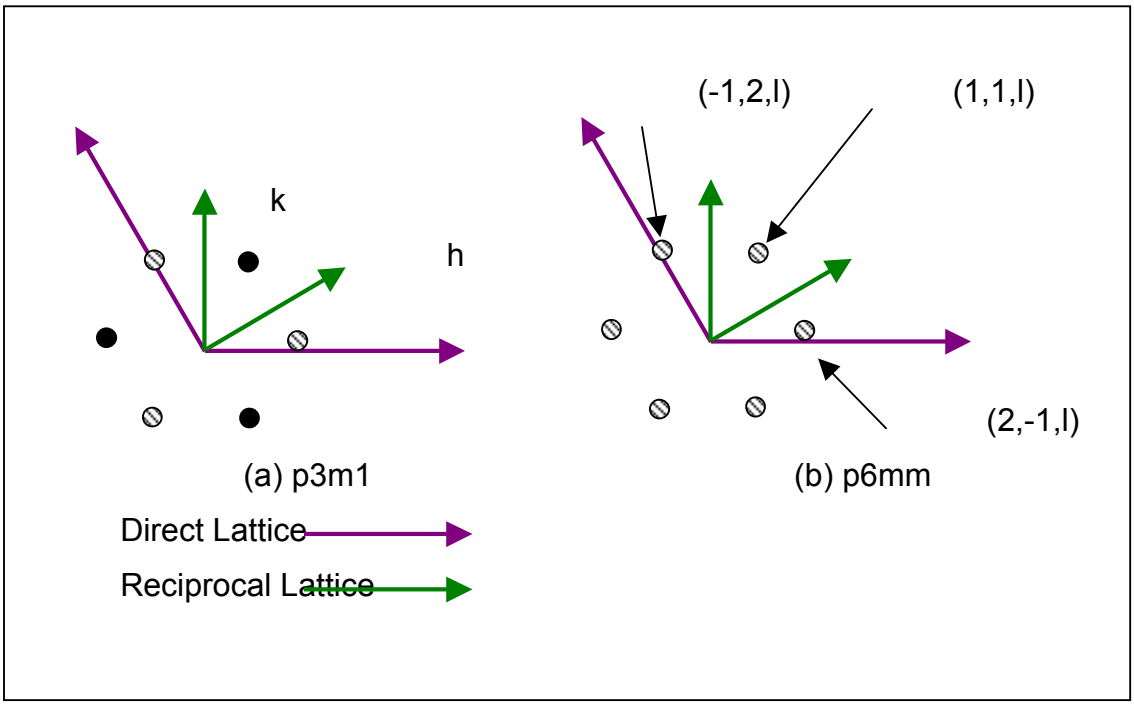

Figure 2-3 Diffraction patterns of p3m1 and p6mm symmetry groups

Due to the three fold symmetry of the p3m1 symmetry group the reflection at (1,1,l) (any value of l) is inequivalent to the reflection (-1,-1, l), while in the case of p6mm symmetry group these reflections are equivalent. It can be shown that if the crystal has inversion symmetry then the diffraction patterns has inversion symmetry too:

$$F(-\vec{q}) = \int \rho(\vec{r}) e^{-i(-\vec{q}\cdot\vec{r})}\, d^3\vec{r}$$

$$\vec{r} \Rightarrow -\vec{r}$$

$$F(-\vec{q}) = -\int \rho(-\vec{r}) e^{-i(\vec{q}\cdot\vec{r})}\, d^3\vec{r}$$

$\rho(\vec{r}) = \rho(-\vec{r})$ by inversion symmetry of the crystal therefore :

$F(-\vec{q}) = -F(\vec{q})$

Since the observed intensity is $|F(\vec{q})|^2$, the diffraction pattern has inversion symmetry. Due to the inversion symmetry of the diffraction pattern, (-1,-1,l) reflection is equivalent to (1,1,-l) reflection. Using the inversion symmetry and the three fold symmetry of the p3m1 symmetry group we can show that (1,1,l) reflection is in-equivalent to the (1,1,-l) reflection. Similarly in the case of p6mm symmetry group we can show that (1,1,l) reflection is equivalent to (1,1,-l) reflection. Figure 2-4 shows the (7,3,l) surface rod measured from Si7x7 reconstructed surface.

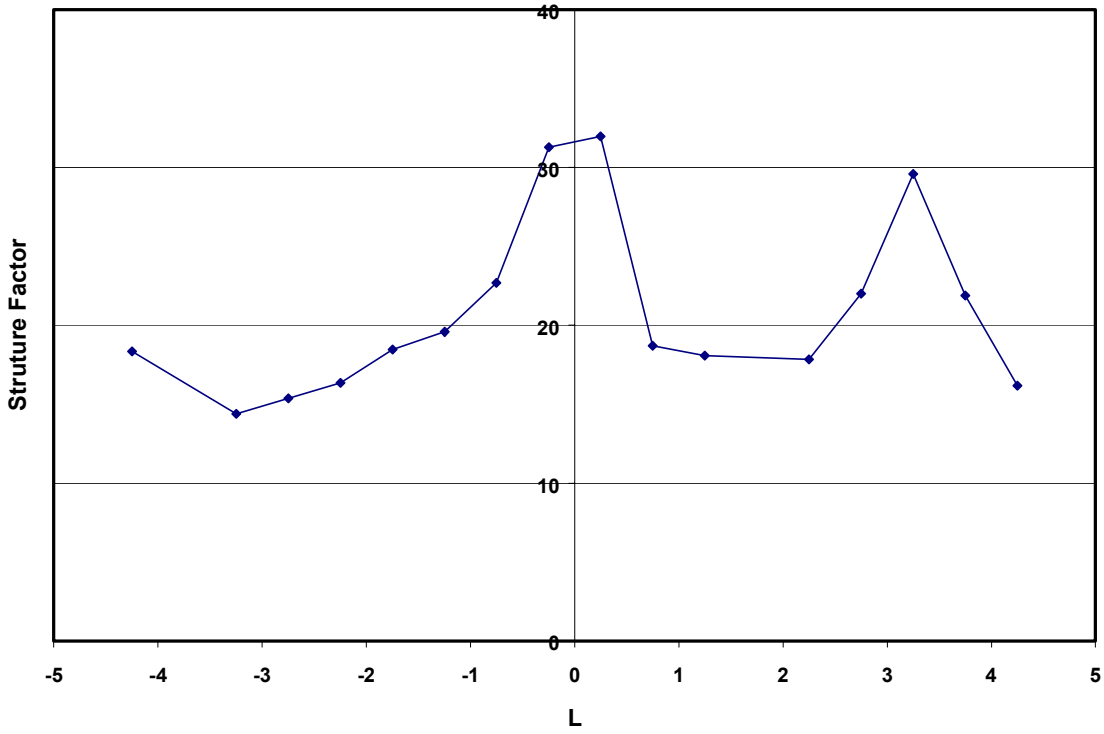

Figure 2-4 (7,3) surface rod from Si7x7(111) surface

In the case of this surface rod (7,3,l) reflection is not equivalent to a (7,3,-l) reflection indicating that the diffraction pattern has a three fold symmetry about the center, counter intuitive to the predicted six fold symmetry by the p6mm symmetry of the DAS model.

To understand and answer this anomaly one needs a good understanding of the three dimensional structure of the Si7x7 reconstruction.

2.4. Experiment

The experiments were conducted at X16A beamline at the National Synchrotron Light Source at the Brookhaven National Labs. This beamline has a 5-circle high-resolution diffractometer for conducting surface x-ray scattering experiments in ultrahigh vacuum. The beamline uses a bent cylindrical mirror to focus bending-magnet radiation onto a $1mm^2$ spot on the sample. The incident beam was monochromated (1.57 Å) by a pair of parallel Si(111) crystals. We used a 6mmX30mm Si(111) sample in this experiment. The sample was first etched to produce a good oxide layer (the oxide is the key to a good 7x7 reconstruction). Then it was flashed to 1200^oC for 5 seconds and cooled very quickly to about 900^oC. From this temperature the sample was slowly cooled to 750^oC. This is the temperature region where the surface forms it's ordered reconstruction. Then from 700^oC it was cooled quickly to the room temperature. The pressure in the chamber during the measurements during the next 84 hours was found to be around $5.2X10^{-10}$ torr. To measure structure factors we did rocking scans (the magnitude of q is kept constant) about each point in the reciprocal space. One has to make sure that the scans are wide enough to allow a background subtraction, which is very important to get a good measure of the structure factor.

The unit cell of the reconstructed surface, as the name suggests, is 7 times larger than the SI(111) unit cell in each in-plane direction. The size of this unit cell are 26.8811 Å by 9.40625 Å. The cubic lattice is reindex as hexagonal to place the perpendicular directrion along the 'z' axis.

2.5. Rocking Scans

Due to the finite size of the crystal the reflections are not infinitesimally sharp and require the analyzer to sample a finite region of the reciprocal space to estimate the structure factor of the reflection. Also due to the finite resolution of the diffractometer it not possible to align the diffractometer perfectly at a reflection. These problems are overcome by performing a rocking scan around

the reflection. During a rocking scan the magnitude of the scattering vector is kept constant.

$$|\vec{q}| = \frac{4\pi}{\lambda}\sin\frac{2\theta}{2} = 2\pi\sqrt{h^2\left|\vec{b}_1\right|^2 + k^2\left|\vec{b}_2\right|^2 + l^2\left|\vec{b}_3\right|^2} = \text{constant}$$

where $\vec{b}_1, \vec{b}_2, \text{and}\, \vec{b}_3$ are the reciprocal lattice vectors.

The rocking scan should be sufficiently large to provide an accurate estimation of the background intensity. The background intensity is subtracted from the scan and the scan is then integrated get an estimate of the structure factor. In a crystal comprising or domains which randomly oriented, and are random in size the shape of the rocking scan is expected to be Lorentzian. The intensity of the peak along the rocking scan is given by:

$$I(\phi) = \frac{1}{\pi}\frac{\frac{1}{2}\Gamma(h,k,l)}{\phi^2 + (\frac{1}{2}\Gamma(h,k,l))^2} + n(\theta,\phi,\chi)$$

where ϕ is one of the Eulerian angles, $\Gamma(h,k,l)$ is the Full Width at Half Maximum of the reflection (h,k,l), and $n(\theta,\phi,\chi)$ is the background noise. The background noise is assumed to be constant over the entire scan, and can be estimated by making the scan sufficiently wide in ϕ. The relationship between the structure factor of the reflection and the observed intensity in the rocking scan are related by:

$$\left|S(h,k,l)\right|^2 = \int_{\phi_{min}}^{\phi_{max}} \left(I(\phi) - n(\theta,\phi,\chi)\right) d\phi$$

Symmetry equivalent structure factors are averaged together to eliminate the effects of small misalignment or any other imperfection of the sample.

2.6. 2D Analysis

The starting point chosen for the purpose data analysis was chosen to be the unrelaxed surface of Si1x1 with the dimer atoms, adatoms, and stacking fault to provide all the necessary components of the DAS model. The structure of the

DAS model has a p6mm as mentioned before. However the relaxation of the atomic positions may not follow this high symmetry. This can be understood by including a bilayer of the bulk below the DAS model. It is expected that the relaxation of the atoms will not confine itself only to the top layer but will also penetrate to other layers below this. Since these layers (bilayers), below the top layer, have a lower symmetry (p3m1) than the top layer the relaxation pattern need not confine itself to the symmetry of the DAS model. This is illustrated in figure 2-5.

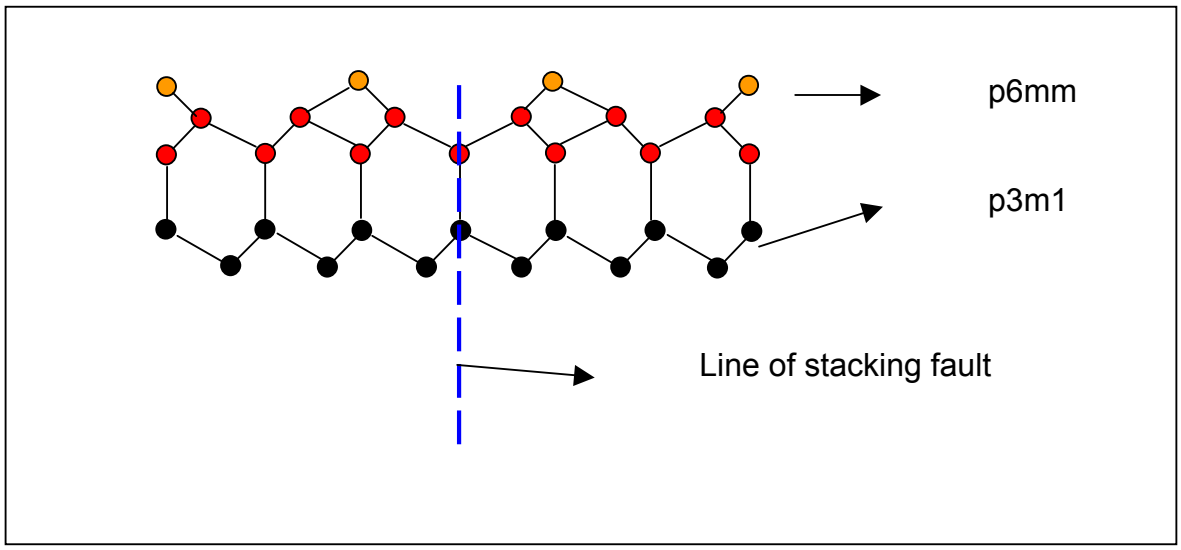

Figure 2-5 DAS model (viewed along the stacking fault)

The atoms of the DAS model are shown in color and the atoms of the bulk are shown in black. The stacking fault in the DAS model makes the two halves of the unit cell symmetric (p6mm) whereas in bulk due to no stacking fault the two halves are not symmetric as seen in the figure. The presence of the bulk layers makes the near neighbor environment of the atoms in the two halves of the unit cell different. Due to this difference in the near neighbor environment it was auumed that the relaxation of the atoms in the two halves of the unit cells will be different though the two halves of the unit cell are symmetric to begin with. This extra degree of freedom that is provided in fitting the data does not bias the model towards a higher symmetry but at the same time it increases the number of fitting parameters.

The chi-square between the data and the calculated structure factors is given by $\chi^2 = \frac{1}{N_{dat} - P}\left(F_{dat}(h,k,l) - F_{calc}(h,k,l)\right)^2$ and is a measure of the goodness of the fit. N_{dat} is the total number of data points and P is the number of fitting parameters. The chi-square is a function of the fitting parameters (displacements of all the atoms and Debye-Waller factors). The best fit of parameters is obtained by minimizing the chi-square.

It can be shown that if the momentum transfer vector has no component in the direction normal to the surface then the structure factors are independent of the position on the atoms in the direction normal to the surface.

$$F(\vec{q}) = \int \rho(\vec{r})\, e^{i\vec{q}\cdot\vec{r}}\, d^3\vec{r}$$

if $q_\perp = 0$ then

$$F(\vec{q}) = \int \rho(x,y,z)\, e^{i(q_x x + q_y y)} dx\, dy\, dz$$

$$= \int \rho^0(x,y)\, e^{i(q_x x + q_y y)}\, dx\, dy$$

where $\rho^0(x,y) = \int \rho(\vec{r})\, dz$ i.e. the projected density

This result is also known as the projection theorem which illustrates that to fit the inplane (x & y) coordinates of the structure one should choose reflections with the momentum transfer vector in the plane of the surface, i.e. L = 0. Due to the limitations of the apparatus it is impossible to measure reflections with L = 0. Reflections at L = 0.2 were used for this purpose. The value of L = 0.2 is sufficiently small for the out of plane coordinates of the atoms to have no significant impact on the fit.

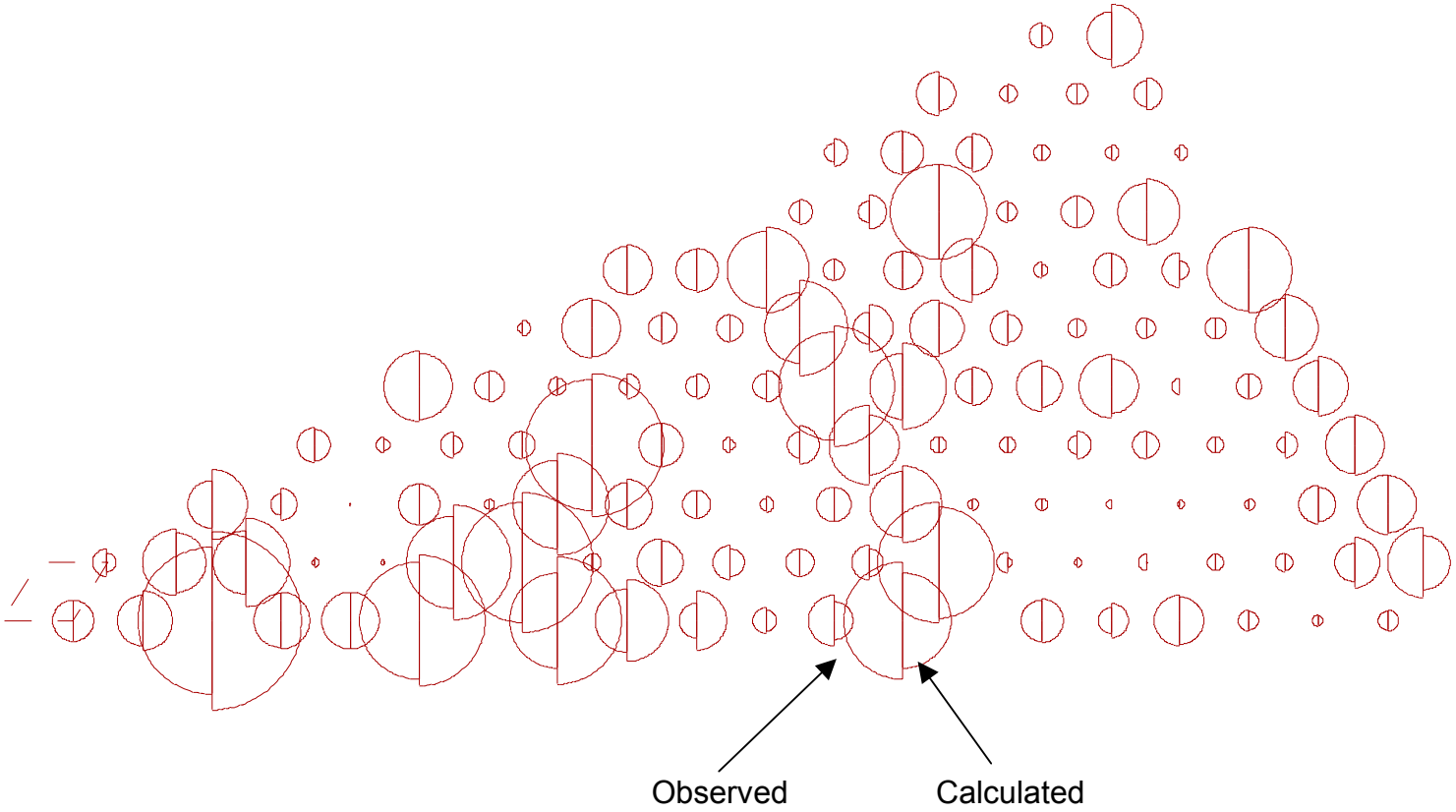

Figure 2-6 Comparison of data and model for in-plane reflections

126 inplane reflections (L = 0.2) were chosen to fit the parameters coupled to the inplane position of the atoms in the model. As mentioned earlier to prevent the model from getting biased towards a higher symmetry the atoms in the faulted and unfaulted halves were allowed to relax independently. Due to this criteria the number of parameters to be fitted to refine the inplane coordinates of the atoms was large (39 parameters) and required such large number of inplane reflections to fit.

One of the most important result of this preliminary 2-D analysis was the dimer bondlengths (2.53 Å $\pm$ 0.04 Å), which is considerably larger than the bulk bondlengths of 2.35 Å. This is a sign of the fact that the surface is tensile stress. Another interesting point to be noticed is a net radial contraction of the trimer of the 2nd layer of atoms adjacent to the adatoms which was 0.132 Å ± 0.05 Å (for the faulted side of the unit cell and 0.119Å for the unfaulted side of the unit cell). These figures compare quite well with the value 0.148 Å obtained by total-energy minimization technique[11, 12]. These results obtained from fitting the inplane coordinates of Si7x7 structure are also in good agreement with previous studies (Robinson et. al. 1986 , Qian and Chadi et. al. 1986 & 1987) (χ^2 = 1.8). The refinement of the inplane (2D) structure provides us with a starting point for the refinement of the 3D structure.

2.7. 3D Analysis

As shown in figure 2-6 for the inplane reflections it was possible to go very far in the (H,K) space (H = 21 & K = 21). However due to the limitations of the diffractometer as one goes towards large L (L = 5) it is not possible to go very far in the (H,K) space. Due to this limitation of the diffractometer the number of reflections available for fitting the 3D structure of the surface model, at large L, were rather limited. The total number of parameters for fitting the 3D structure were 59 (including the Debye-Waller factors). Due to this large number of parameters the fit was unstable. To improve the stability of the fit additional criteria were generated using the concept of Keating energy (P. N. Keating 1966)

2.8. *Keating Energy*

The concept of Keating energy is used for determination of eleasticity, cohesive energy and lattice dynamics of crystals. Choosing a proper expression for the total energy, caused by distortion of the solid, is at the heart of such an analysis. The energy is subjected to various physical requirements and these can be divided into two classes: the general conditions such as translational and rotational invariance and those imposed by the symmetry of the crystal. Without any loss of generality one can assume that the total energy depends only on the position of the nucleii. This assumption is quite true for non-metallic crystal even when the electrons are treated in detail since the Born-Oppenheimer approximation ensures that the electrons follow the nuclei in full.

However the requirement of translational invariance can be met only if the total energy is only a function of the difference between nuclear position.

$$V = V(\vec{r}_k - \vec{r}_l) = V(\vec{r}_{kl})$$

This expression does meet the criteria of translational invariance but fails to meet the criteria of rotational invariance since $\vec{r}_{kl}$ transform like vectors and are not invariant under rotation. One such invariant quantity that can generated from $\vec{r}_{kl}$ is their scalar products

$\theta_{klmn} = \left(\vec{r}_{kl} \cdot \vec{r}_{lm} - \vec{R}_{kl} \cdot \vec{R}_{mn}\right)$ where $\vec{R}_{kl} = \vec{R}_k - \vec{R}_l$ and $\vec{R}_k$ is the position of the k^{th} atom in the undistorted solid. The last term in θ_{klmn} is introduced to make sure that the total energy vanishes if the solid is not subjected to any distortion.

Since θ_{klmn} are small higher order terms in the Taylor series expansion of V can be ignored. The constant term in such an expansion must vanish since if the solid is undistorted then the energy is zero. Also to ensure that the energy is an extremum the linear term must vanish too. Thus the highest order of contribution is from the quadratic term from the Taylor expansion.

$$V = \frac{1}{2} B^{klmn}_{pqrs}\ \theta_{klmn} \theta^{pqrs} \quad + \quad O(\theta^3)$$

The number of terms in such an expression is very large however they are not all independent or important as can be seen in the next section.

In covalent crystals like Si or C the distortion which extends or contracts the bond between two atoms costs more energy than distortion which causes bending of the bonds. Bending of bond couples to terms like θ_{klmn} where ($k \neq m$ & $l \neq n$), whereas contraction of bond couples to terms like θ_{klkl}. Also using the same argument terms coupling atoms which are not neighbors (no bond exists between them) the important terms in the expansion of the energy can be further reduced to

$$V = \tfrac{1}{2} C_{kl} (\theta^{kl})^2$$

Where $\theta_{kl} = \theta_{klkl}$. Since terms which couples non-neighboring atoms are unimportant this further enforces the condition that k & l are neighbors and m and n are neighboring atoms. Thus in covalent solids the most important contribution to the Keating energy is from the stretching and contraction of bonds. There are further constraints imposed on the Keating energy due to the symmetry group of the crystal. However in our case, as mentioned earlier, the relaxation of the atoms are compliant with the symmetry group thus the Keating energy of the form $V = \tfrac{1}{2} C_{kl} (\theta^{kl})^2$ is invariant under such operations of the symmetry group.

The Keating energy is incorporated in to the fitting algorithm by modifying the chi-square,

$$\chi^2 = \frac{1}{N_{dat} - P} \sum \left(F_{dat}(hkl) - F_{calc}(hkl)\right)^2 + \frac{\Lambda}{N_{bond} - P} \sum_j \sum_i \kappa_{ij} \left(\left| \vec{r}_i - \vec{r}_j \right| - d_{ij} \right)^2$$

Where i, and j are neighboring atoms, and d_{ij} is the bulk bondlength and κ_{ij} is a weighting factor.

Where i, and j are neighboring atoms and d_{ij} is the ideal bulk bondlength and κ_{ij} is a weighting factor associated with each bond. The weighting factor allows us to put smaller weight to the bondlength of the surface atoms than the atoms in the bulk. This is reasonable since at the surface the equilibrium bondlength may differ from that of the bulk. This weight is smallest for the adatoms and increases as we go deeper into the surface.

The stability of the fit improved significantly by including the Keating energy. However the model still failed to match the observed assymetry of certain surface rods in the data and the best fit yielded a chi-squared of 2.75. It was believed at this point that it is very crucial to include the anharmonicity of the vibration of surface atoms into the model. As mentioned earlier we expect the effects of anharmonicity to be more prominent at the surface than in the bulk

2.9. Anharmonic Debye-Waller Factors

In the previous chapter the concept of Debye-Waller factor was introduced as means of incorporating thermal vibrations of the atomic nuclei in x-ray scattering. We have extended this concept to include vibrations due to anharmonic interatomic potentials.

The majority of the contribution to the atomic form factor is due to the core electrons. In non metallic solids it is valid to assume that the vibration of the core electrons will follow that of the nuclei (Born-Oppenheimer approximation). The atomic form factor is given by,

$$f(q) = \int \rho(\vec{r}) e^{i(\vec{q}\cdot\vec{r})} d^3\vec{r}$$

Where $\vec{r} = \vec{R} + \vec{u}$, $\vec{R}$ is a Bravais equilibrium lattice position and $\vec{u}$ is the displacement of the atom from the Bravais lattice position. This displacement can be due to defects, relaxation and most important of all thermal vibration. The density function is a convolution of the density of the electrons around the nuclei with the probability distribution function of the atom due to vibration.

$$\rho(\vec{r}) = \rho_1(\vec{R}) \otimes \rho_2(\vec{u})$$

Thus the form factor can be expressed as

$f(\vec{q}) = f''(\vec{q})T(\vec{q})$, where $f''(\vec{q})$ is the form factor in absence of thermal vibration and $T(\vec{q})$ is the effect of thermal vibration. In case of a harmonic interatomic potential the probability distribution function is a simple Gaussian,

$$\rho_2(\vec{u}) = \frac{1}{(2\pi)^{\frac{3}{2}}} e^{-\sum_{i=1}^{3} \frac{u_i^2}{2\sigma_i}}$$

It can be shown that for such a case the contribution of thermal vibrations to the Debye-Waller factor is

$T(\vec{q}) = e^{-2M}$, where $M = \frac{1}{4}\left\langle (\vec{q}.\vec{u})^2 \right\rangle$ (Debye 1913, Waller 1923).

It has been shown that in case of anharmonic interatomic potential the probability distribution function can be expressed as,

$$\rho_{2\,anh}(\vec{u}) = \rho_{2\,har}(\vec{u})\left[1 - C^{i}D_i + \tfrac{1}{2!}C^{ij}D_iD_j - \tfrac{1}{3!}C^{ijk}D_iD_jD_k + \tfrac{1}{4!}C^{ijkl}D_iD_jD_kD_l + ...\right]$$

where C^{i}, C^{ij}, C^{ijk} are tensorial coefficients and $D_i = \frac{\delta}{\delta u_i}$. Thus the probability distribution function for an anharmonic interatomic potential is a differential expansion of the harmonic probability distribution function. The first and the second differential term in the expansion represent the change in the mean position and the change in the standard deviation respectively. This can be easily seen by

$e^{-\frac{(u+\delta u)^2}{2(\sigma+\delta\sigma)}} = e^{-\frac{1}{2}(u+\delta u)^2\left(\frac{1}{\sigma}-\frac{\delta\sigma}{\sigma^2}\right)} = e^{-\frac{u^2}{2\sigma}}\left(1 + \frac{1}{2\sigma}u\,\delta u - \frac{\delta\sigma}{2\sigma^2}u^2\right)$. Thus these terms are unimportant and can be eliminated from the expression since refinement of the positions and the standard deviation are done separately in the fitting algorithm.

$$\rho_{2\,anh}(\vec{u}) = \rho_{2\,har}(\vec{u})\left[1 - \tfrac{1}{3!}C^{ijk}D_iD_jD_k + \tfrac{1}{4!}C^{ijkl}D_iD_jD_kD_l + ...\right]$$

The anharmonic Debye-Waller factor is the Fourier Transform of this function.

$$T_{anh}(\vec{q}) = T_{har}(\vec{q})\left[1 - \tfrac{1}{3!}C^{ijk}q_iq_jq_k + \tfrac{1}{4!}C^{ijkl}q_iq_jq_kq_l + ...\right]$$

Where $T_{har}(\vec{q}) = e^{-2M}$ the traditional Debye-Waller factor. The tensorial coefficients C can be related to the anharmonic parameters of the interatomic potential. In our study we consider the interatomic potential to be of the form.

$$V(\vec{u}) = V_{har}(\vec{u}) + \gamma^{ijk}u_iu_ju_k + \delta^{ijkl}u_iu_ju_ku_l$$

The relation between the tensorial coefficients and the parameters of the interatomic potential can be solved by solving the Schroedinger equation for the anharmonic probability distribution function.

$$-\sum \frac{1}{2m}\frac{\delta^2}{\delta u_i^{\,2}}\rho_{har}(\vec{u})\left[1-\tfrac{1}{3!}C^{ijk}u_iu_ju_k+...\right]$$
$$+\left[V_{har}(\vec{u})+\gamma^{ijk}u_iu_ju_k+\delta^{ijkl}u_iu_ju_ku_l\right]\rho_{har}(\vec{u})\left[1-\tfrac{1}{3!}C^{ijk}u_iu_ju_k+...\right]$$
$$=E\rho_{har}(\vec{u})\left[1-\tfrac{1}{3!}C^{ijk}u_iu_ju_k+...\right]$$

Solving this equation and matching terms of same order we get

$C^{ijk}=-i\gamma^{ijk}$, $C^{ijkl}=\delta^{ijkl}$, $C^{ijklm}=0$, $C^{ijklmn}=\gamma^{ijk}\gamma^{lmn}$ etc.

Using these results and applying them to the expression for $T_{anh}(\vec{q})$ we get

$$T_{anh}(\vec{q})=e^{-2M}\exp(-i\gamma^{ijk}q_iq_jq_k+\delta^{ijkl}q_iq_jq_kq_l)$$

As can be seen from the expression inclusion of anharmonicity in interatomic potential increases the total number of parameters drastically since there are 27 γ^{ijk} and 81 δ^{ijkl}. It turns out that not all of these are important. We assume the anharmonicity of the interatomic potential is prominent only in the direction normal to the surface, i.e.

$$V_{anh}(\vec{u})=V_{har}(\vec{u})+\gamma^{333}(u_3)^3+\delta^{3333}(u_3)^4.$$

The anharmonicity in the inplane direction is considered to be negligible. Under these assumption the modified Debye-Waller factor can be simplified as

$$T_{anh}(\vec{q})=e^{-2M}\exp(-i\gamma^{333}(q_\perp)^3+\delta^{3333}(q_\perp)^4)$$

By including anharmonic terms in the Debye-Waller factor the fit could be considerable improved and the resulted in a chi-squared of 2.175.

2.10. Results and Conclusion

We report first a 2-D structural analysis to get an idea of the in-plane structure of the surface. We used in-plane reflection ($q_\perp$ = 0.25 in normalized units) for this purpose. The unrelaxed Si7X7 surface with the dimer, adatoms and the stacking fault was chosen to be the starting model. As used by Pederson[**]

(Sn/Ge111), a bilayer of the bulk Si was added to Takayanagi's model since we expect the surface strain field to penetrate into the bulk. The attributed p6mm symmetry of the surface is a key point of this investigation so we decided to let our fitting model have a lower symmetry namely p3m1. There is no distinction between the p6mm symmetry and p3m1 symmetry for the in-plane data ($q_\perp = 0$) but since the measurements were done at $q_\perp = 0.25$ some effect of the broken symmetry is expected to be seen. Thus the atoms on the two halves of the 7x7 unit cell are allowed to relax independently. This gave 17 fitting parameters for the in-plane fit. Adding the bilayer of the bulk result in another 22 fitting parameters for the in-plane fit, a total of 39 parameters altogether. This model was fitted against 125 in-plane reflection. Method of least-squares was used to fit the model to the experimental data which yielded in a $\chi^2 = 2.05$. Figure 2 shows a comparison between the experimental data and the results of the in-plane fit. One of the most important result of this preliminary 2-D analysis was the dimer bondlengths (2.53 Å $\pm$ 0.04 Å), which is considerably larger than the bulk bondlengths of 2.35 Å. This is a sign of the fact that the surface is tensile stress. Another interesting point to be noticed is a net radial contraction of the trimer of the 2nd layer of atoms adjacent to the adatoms which was 0.132 Å ± 0.05 Å (for the faulted side of the unit cell and 0.119Å for the unfaulted side of the unit cell). These figures compare quite well with the value 0.148 Å obtained by total-energy minimization technique[11, 12]. Both of these results are in good agreement with results obtained from previous X-ray diffraction studies[3].

The fit of the model to the in-plane data was used as a starting point for the 3D structure. To begin with the model was fit to the 7x7 surface rods (no contribution form the truncated bulk). The additional degree of freedom increases the total number of parameters to 55 which is a rather large number for fitting since we had only 25 nonequivalent surface rods with a total of 189 measurement points. The model was fitted simultaneously to the in-plane and out of plane reflection. Adding the two sets of data gives a total 289 measurements to fit, which should be sufficient to determine all parameters, but it also gives rise to instability in the fit. To avoid the instability some restrictions were imposed on

the bond length. The bond lengths were constrained to be close to the bulk Si bondlength (2.35 Å). The retrictions on the bond length were not applied to the adatoms and the dimers. The previously used expression for χ^2 is

$$\chi^2 = \frac{1}{N_{dat} - P} \sum \left(F_{dat}(hkl) - F_{calc}(hkl)\right)^2$$

Where N_{dat} is the number of data points and P is the number parameters to be fitted

To this expression of χ^2 we added the bond length constraints

$$\chi^2 = \frac{1}{N_{dat} - P} \sum \left(F_{dat}(hkl) - F_{calc}(hkl)\right)^2 + \frac{\Lambda}{N_{bond} - P} \sum_j \sum_i \kappa_{ij} \left(\left|\vec{r}_i - \vec{r}_j\right| - d_{ij}\right)^2$$

Where i, and j are neighboring atoms, and d_{ij} is the bulk bondlength and κ_{ij} is a weighting fa

The weighting factor increases as one goes deeper towards the bulk from the surface and at the surface the weighting factor is '0' for the adatoms and the dimers. Λ is an overall weighting factor of the constraints due to the bondlength restriction with respect to the constraints due to the structure factor fit. This constraint is very similar in expression and principle of minimizing the Keating energy[16].

By adding these artificial constraints simultaneously with the crystallographic data the fit could be stabilized. One of the most important results of this fit was that the displacements of the adatoms normal to the surface were different for the unfaulted and the faulted halves of the unit cell. In fact for most of the atoms in the first three layers of the surface we see this effect, but it is most prominent for the adatoms. The displacements in the faulted halves are more then the displacements in the unfaulted half. The average out of plane displacements for the adatoms in the unfaulted half of the unit cell is 0.448 Å ±0.034 Å relative to it's ideal position in the Si bulk unit cell. Compared to that of the unfaulted half of the unit cell which is 0.181 Å ± 0.022 Å. These displacements which may seem very large at first can be understood as a stress relieving mechanism. The adatom in the unrelaxed state as shown in figure 4 is very close to the atom directly below it and the separation is smaller than the bond length of bulk Si. This causes the adatom to be pushed outwards in the perpendicular direction. The relaxation of the adatom, leads to a net inward

contraction of the trimer of atoms as shown in figure 4. The inward contraction of the trimers relieves elastic strain of the surface. As the trimers contract in the two halves of the 7x7 unit cell it produces a dislocation along the line separating the two halves. This being dislocation is filled with a chain of dimer atoms (figure 4) .

This result indicates that the planar symmetry of the 7X7 surface (p6mm) is broken by the atoms in the two halves of the 7x7 cell being different. As one goes to smaller and smaller $q_{\perp}$ in the reciprocal space the effects of the broken symmetry vanishes and the in-plane structure is unable to differentiate between p6mm and p3m1 symmetry groups. A surface with p6mm symmetry would have the fractional orders rods[21] (1, 3/7) and (-1, -3/7) identical because of the 6 -fold symmetry of the surface. Figure 5 shows a comparison of these two surface rods. Inversion symmetry is used to project the (-1, -3/7, L) rod onto the (1, 3/7, -L) rod and one can see that the symmetry is 3-fold. This broken symmetry is seen in other surface rods too, but less prominent. The reason for the (1, 3/7, L) rod to show such strong asymmetry is the fact that the strongest contribution to this rod comes from the adatoms and the adatoms show the largest dergree of assymetry in relaxation in the two halves of the unit cell.

The fit for this surface rods is still unable to explain the large asymmetry in the (1, 3/7, L) rod, though the difference in the relaxation of the adatoms in the two halves does give rise to a certain amount of asymmetry in the fractional order surface rod. It is also very difficult to explain the observed difference in the relaxation of the adatoms in the two halves. Results from energy calculations[12, 13], have shown any significant difference in the bondlength of the Si atoms between the normal and the faulted stacking and which also means that one expects similar amount of relaxation for the atoms in the faulted and the unfaulted parts of the unit cell. However the total energy calculations ignore excitations since they are at T = 0.

This assymetry of the diffraction pattern can be explained by considering anharmonic terms in the interatomic potential between the Si atoms. The Debye Waller factor for the structure factor is evaluated using a perfectly harmonic interatomic potential. This assumption holds true for the atoms several layers into

the bulk, but for the atoms near the surface, specially the adatoms, this is not the case. Due to the truncation of the crystal one expects third and fourth order terms to play a more significant role in the interatomic potential than they would in the bulk. Debye-Waller factor, which arises because of thermal vibration of the scattering electronic core about the minimum of the interatomic potential, is the Fourier transform of the probability distribution function (pdf) of the scattering core. In case of a harmonic interatomic potential the probability distribution function (pdf) is a simple gaussian which leads to a Debye-Waller factor of the form $D = e^{-2M}$ where $M = \frac{1}{4}\left\langle (\vec{q}\cdot\vec{u})^2 \right\rangle$, (the average of the square of the displacement along the momentum transfer vector $\vec{q}$). To incorporate the effect of third and fourth order terms in interatomic potential we first found the pdf for such a case and then the Debye-Waller factor is evaluated by taking the Fourier transform of the pdf. In case of interatomic potentials where the third and fourth order terms play a significant role the Debye-Waller factor is $e^{-2M}\,\mathbf{exp}\left[-i\gamma^{ijk}q_i q_j q_k + \delta^{ijkl}q_i q_j q_k q_l\right]$ where the coefficients γ and δ are the third and fourth order coefficients of the interatomic potential respectively, given by:

$$V(\mathbf{r}) = V_{harmonic}(\mathbf{r}) + \gamma^{ijk} r_i \quad r_j \quad r_k + \delta^{ijkl} r_i \quad r_j \quad r_k \quad r_l .$$

This expression for the Debye-Waller factor is derived for a very general case. In the current analysis the interatomic potential is assumed to be of the form:

$$V(\vec{r}) = V_{harmonic}(\vec{r}) + \gamma^{333} \quad r_3 \quad r_3 \quad r_3 + \delta^{3333} \quad r \quad {}_3 r_3 \quad r_3 \quad r_3$$

The index ‘3’ represents the direction normal to the surface. At this point we are making an approximation that the third and the fourth order terms are significant only with respect to the direction normal to the surface. Hence the Debye-Waller factors is:

$$e^{-2M} \quad \mathbf{exp}\left[-i\gamma^{333}(q_3)^3 + \delta^{3333}(q_3)^4\right]$$

The ‘γ‘ ‘δ‘ which are properties of the interatomic potential are also treated as fitting parameters. The 3rd and 4th order terms, for the potential, was introduced in the fit only for the adatoms and the atoms on the first layer of the

surface. Table 1 shows the list of all the parameters and the 3rd and 4th order coefficients for the potential are shown at the end of the table. The results of the fit for a few surface and truncation rods are shown in figure 5 to figure 10. The most significant result from this is the difference in the 3rd order coefficient (γ) for the adatoms in the faulted and unfaulted halves of the unit cell. γ for the unfaulted side of unit cell is -0.0056 ($\pm$ 0.067) (normalized to unit cell coordinates) and γ for the faulted side of the unit cell is 0.0846 ($\pm$ 0.058). This difference in the 3rd order (γ) coefficient can explain the difference between the calculated relaxation for the adatoms in these two sides which we talked about before. The expectation value of the position of an atom is $\Delta r + < u >$. Where Δr is the relaxation of the atom from the starting model and $< u >$ is the expectation value of the about this relaxation. In case of harmonic interatomic potential $< u >$ is '0', but due the presence of the 3rd order (γ) terms in the potential it is no longer so. One can calculate $< u >$ by the relation

$< u > =$

$$\int \rho(u) \quad u \quad du = \int T(q) \qquad dq \int e^{iqu} \qquad du = \int e^{-2M} (\exp(i\gamma q^3 + \delta q^4)/q) dq$$

This expression was evaluated by the method of numerical integration and the results are as follows:

$< u >$ for unfaulted half = 0.0012

$< u >$ for faulted half = -0.0237 (in normalized coordinated).

Adding these results for $< u >$ to the relaxation for the adatoms

Unfaulted

$\Delta r + < u >$ (expected position w.r.t starting model) = 0.0205 ± 0.00164

$= 0.1928 \pm 0.015424$ Å

Faulted

$\Delta r + < u >$ (expected position w.r.t starting model) = 0.0239 ± 0.002629

$= 0.2248 \pm 0.024728$ Å

In conclusion the reason for observing a three fold symmetric diffraction pattern is attributed to a difference in the anharmonic coefficients of the atoms

(mainly adatoms) in the two halves of the Si(111)7x7 unit cell. The difference, in the height of the atoms in the tow halves of the unit cell, is found not to be significant (0.03 Å for adatoms) and may explain why other methods like total energy calculation do not show it.

The authors would like to thank the staff of the NSLS Brookhaven National Laboratories, for all their help during the entire course of this study.

Table 1 List of fitted parameters

Parameter	Keating	Keating + Anharmonicity
Scale	0.22569	0.2467
Roughness	0.2884	0.1418
Surface fraction	0.0642	1
Interface distance	N/A	0
Displacement parameter 1	-0.000493	-0.005366
Displacement parameter 2	0.001244	0.00228
Displacement parameter 3	0.004443	0.005006
Displacement parameter 4	-0.000191	-0.000234
Displacement parameter 5	-0.005875	-0.00543
Displacement parameter 6	-0.00716	-0.008038
Displacement parameter 7	-0.003198	-0.003466
Displacement parameter 8	0.005977	0.005562
Displacement parameter 9	0.006428	0.00621
Displacement parameter 10	-0.003037	0.001812
Displacement parameter 11	0.000449	0.000616
Displacement parameter 12	0.022123	0.022785
Displacement parameter 13	-0.022818	-0.023903
Displacement parameter 14	0.023697	0.022649
Displacement parameter 15	-0.004184	-0.004184
Displacement parameter 16	-0.000148	0.000231
Displacement parameter 17	-0.001431	-0.002794
Displacement parameter 18	0.002492	0.002345
Displacement parameter 19	-0.003652	-0.003823
Displacement parameter 20	0.003471	0.004632
Displacement parameter 21	0.004063	0.003996
Displacement parameter 22	-0.002389	-0.003645
Displacement parameter 23	-0.001739	-0.002241
Displacement parameter 24	-0.003417	-0.003076
Displacement parameter 25	-0.000824	-0.001243
Displacement parameter 26	-0.000279	-0.000462
Displacement parameter 27	0.00078	0.000946
Displacement parameter 28	0.00017	0.000856
Displacement parameter 29	-0.001909	-0.001874
Displacement parameter 30	-0.000108	-0.000349
Displacement parameter 31	-0.000271	-0.000035
Displacement parameter 32	0.000911	0.000839
Displacement parameter 33	0.002068	0.001476
Displacement parameter 34	0.005992	0.007496
Displacement parameter 35	0.00309	0.002376
Displacement parameter 36	0.001541	0.000652
Displacement parameter 37	0.000139	-0.000194
Displacement parameter 38	-0.001663	-0.003164
Displacement parameter 39	-0.001233	-0.00169
Displacement parameter 40	0.121084	0.019325

Displacement parameter 41	0.120962	0.047646
Displacement parameter 42	0.0177	0.017445
Displacement parameter 43	0.024399	0.030434
Displacement parameter 44	-0.032978	-0.042576
Displacement parameter 45	0.019825	0.012552
Displacement parameter 46	-0.030792	-0.028616
Displacement parameter 47	0.003916	0.00168
Displacement parameter 48	0.00019	-0.005455
Displacement parameter 49	0.015991	0.018874
Displacement parameter 50	0.006341	0.014861
Displacement parameter 51	0	0
Displacement parameter 52	-0.010123	-0.059207
Displacement parameter 53	-0.009634	-0.063478
Displacement parameter 54	0.02172	0.031312
Displacement parameter 55	-0.005591	-0.082735
Debye Waller 1	3.1	8.928194
Debye Waller 2	2.6	-0.849113
Debye Waller 3	1.8803	2.194527
Debye Waller 4	0.497	10.63817
Debye Waller 5	1.2	17.29307
Debye Waller 6	N/A	41.36586
Debye Waller 7	N/A	33.935543
Debye Waller 8	N/A	0.5
Debye Waller (3rd) 1	N/A	-0.005688
Debye Waller (3rd) 2	N/A	0.084617
Debye Waller (3rd) 3	N/A	0.037536
Debye Waller (3rd) 4	N/A	0.050124
Debye Waller (4th) 1	N/A	0.041151
Debye Waller(4th) 2	N/A	0.039178
Debye Waller (4th) 3	N/A	-0.021707
Debye Waller (4th) 4	N/A	-0.027632

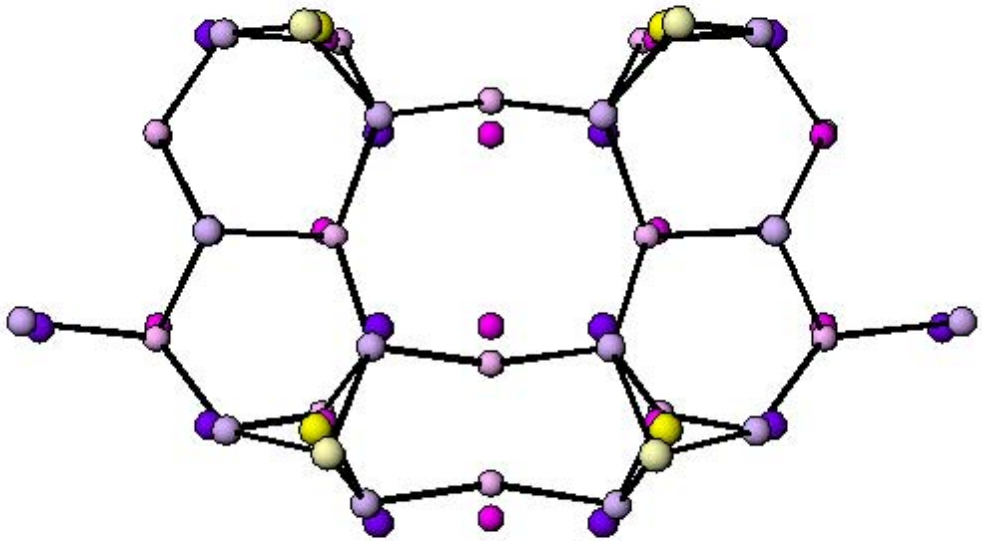

Figure 2-7 Comparison of results and DAS model . The atoms in lighter shade represent the calculated position of the atoms

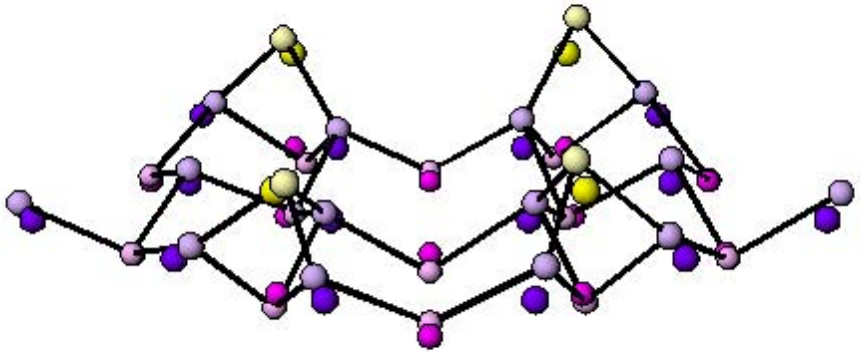

Figure 2-8 Another view of the comparison of results and DAS model

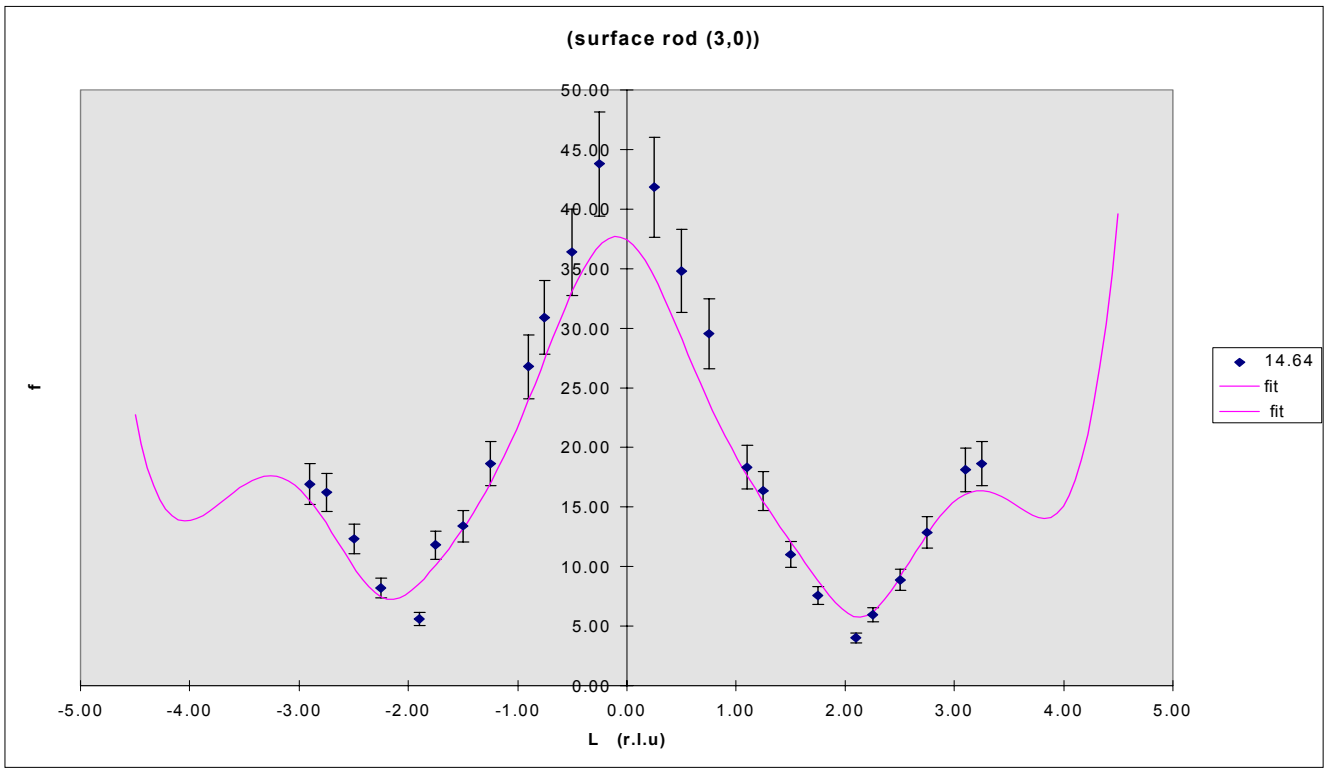

Figure 2-9 (3,0) surface rod

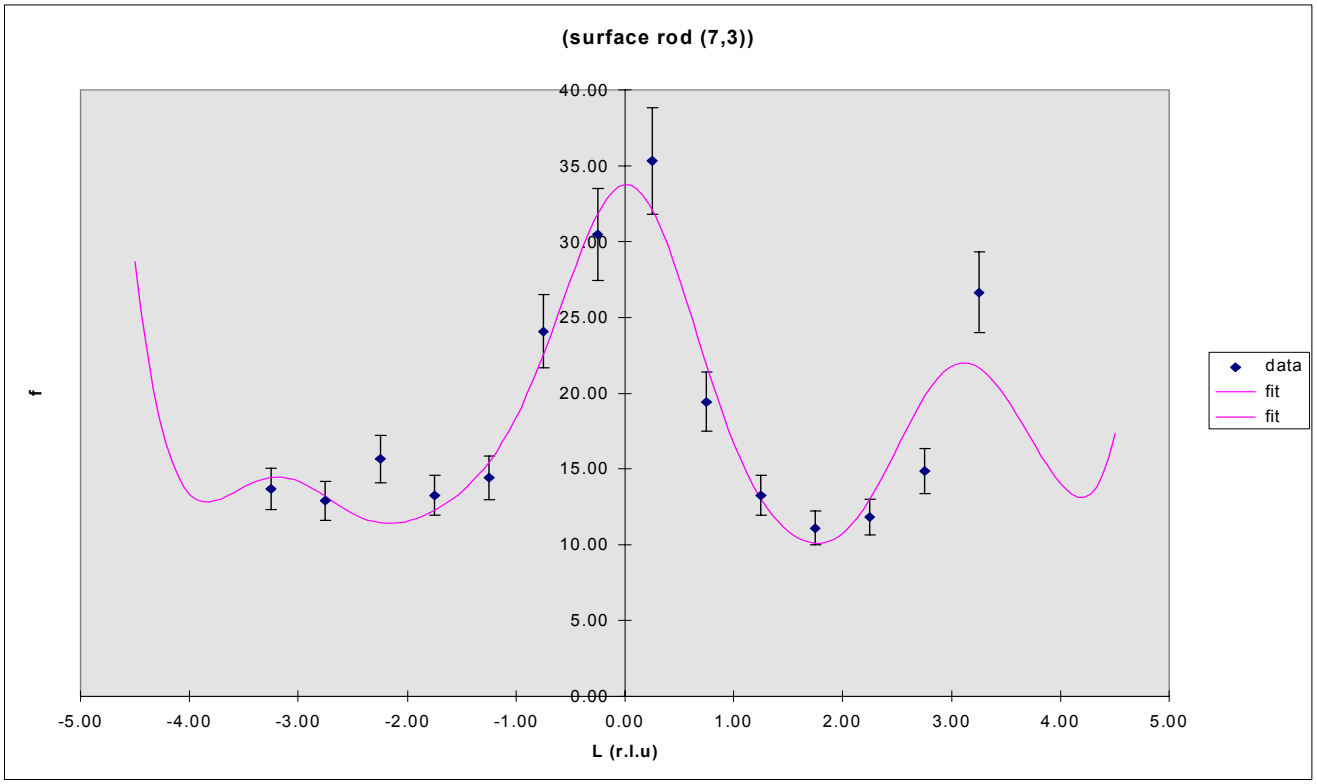

Figure 2-10 (7,3) surface rod

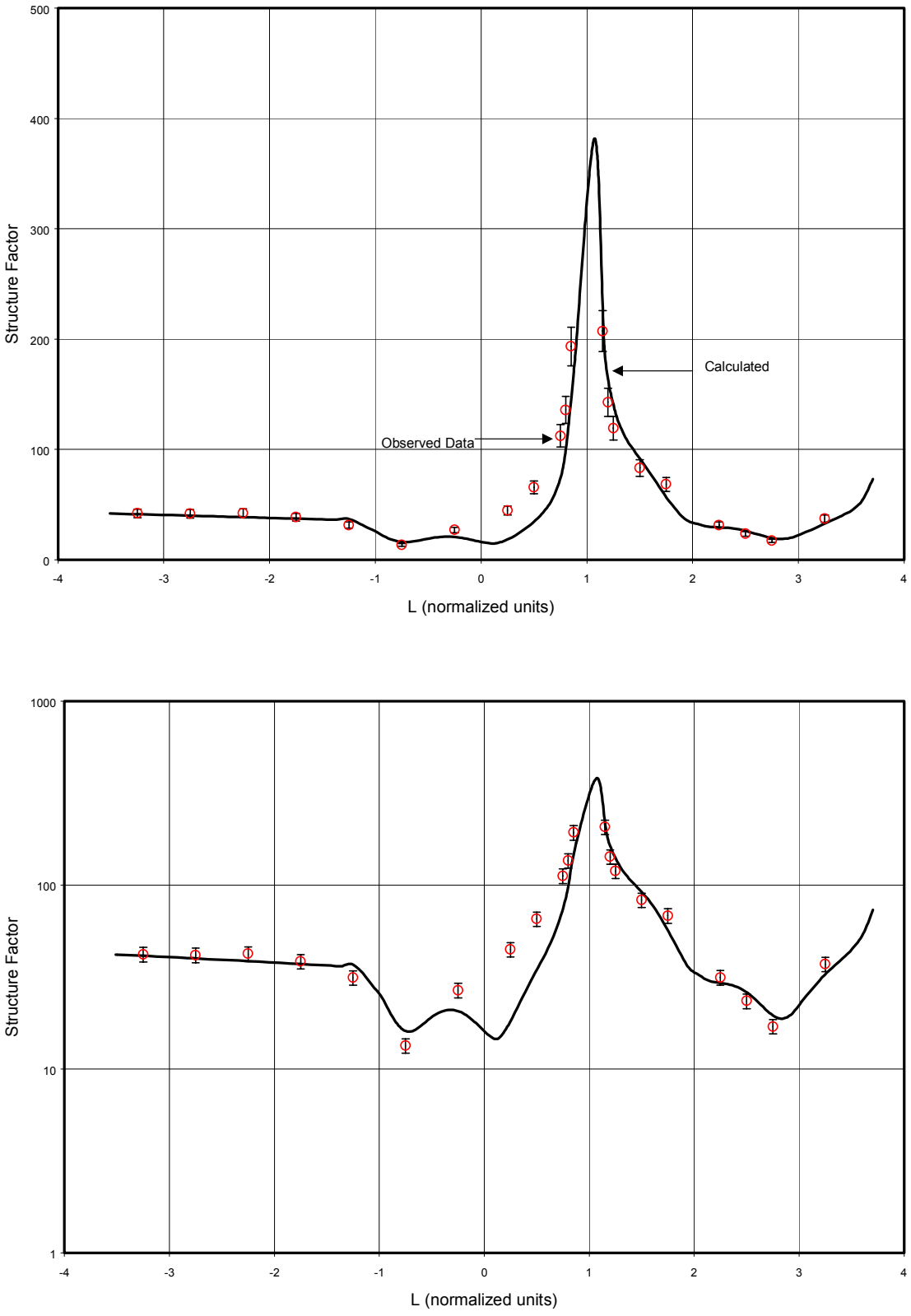

Figure 2-11 (7,0) CTR (crystal truncation rod)

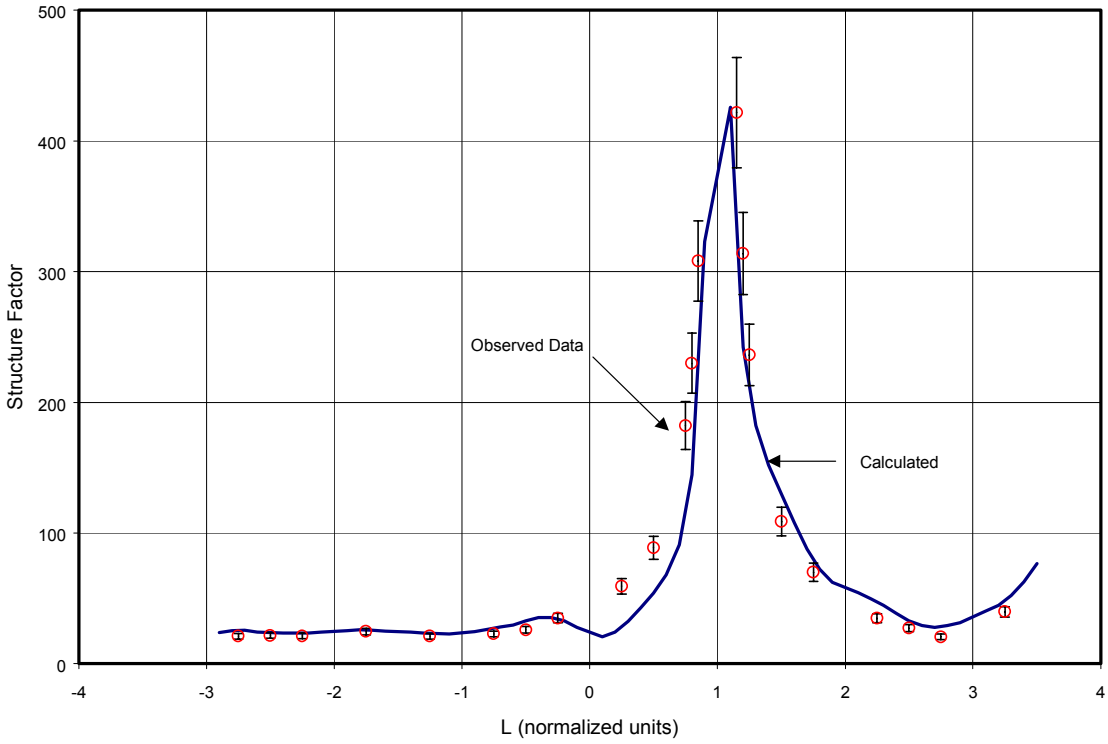

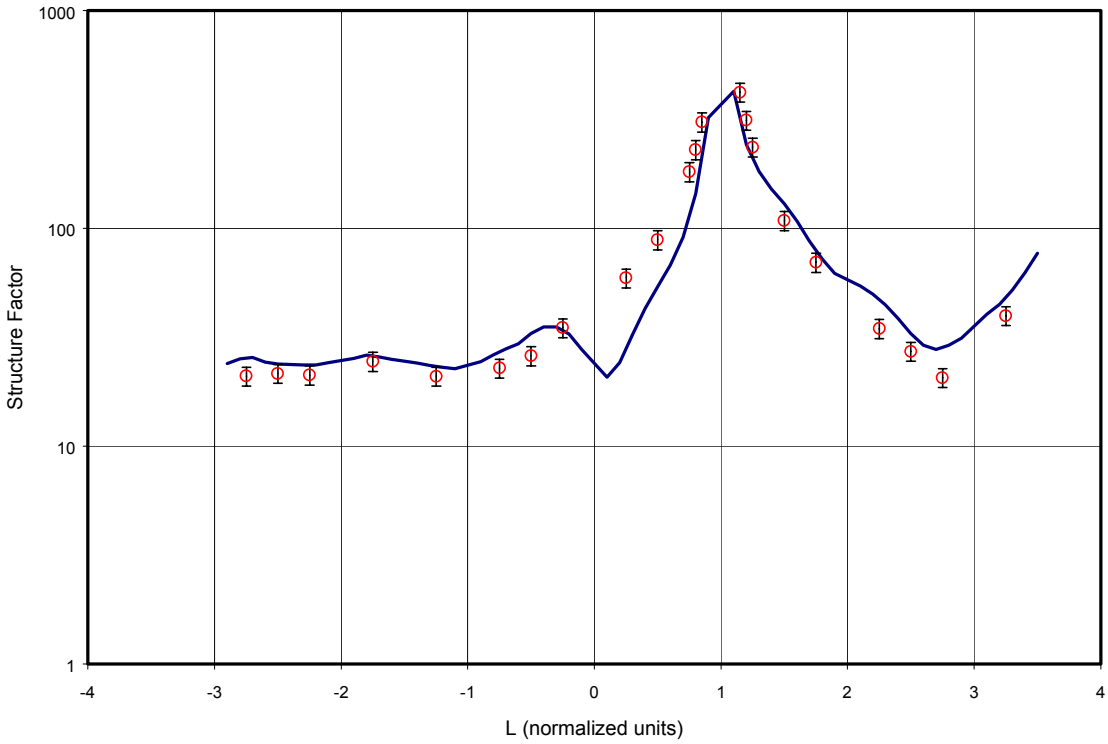

Figure 2-12 (-14, 0) CTR

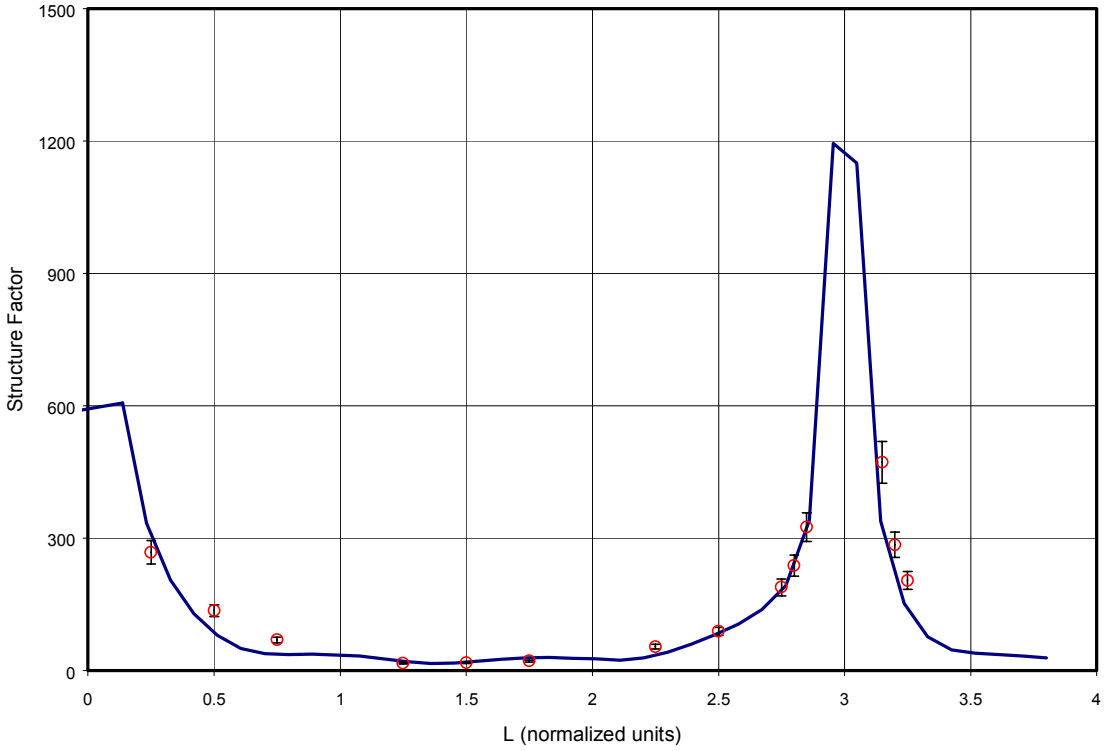

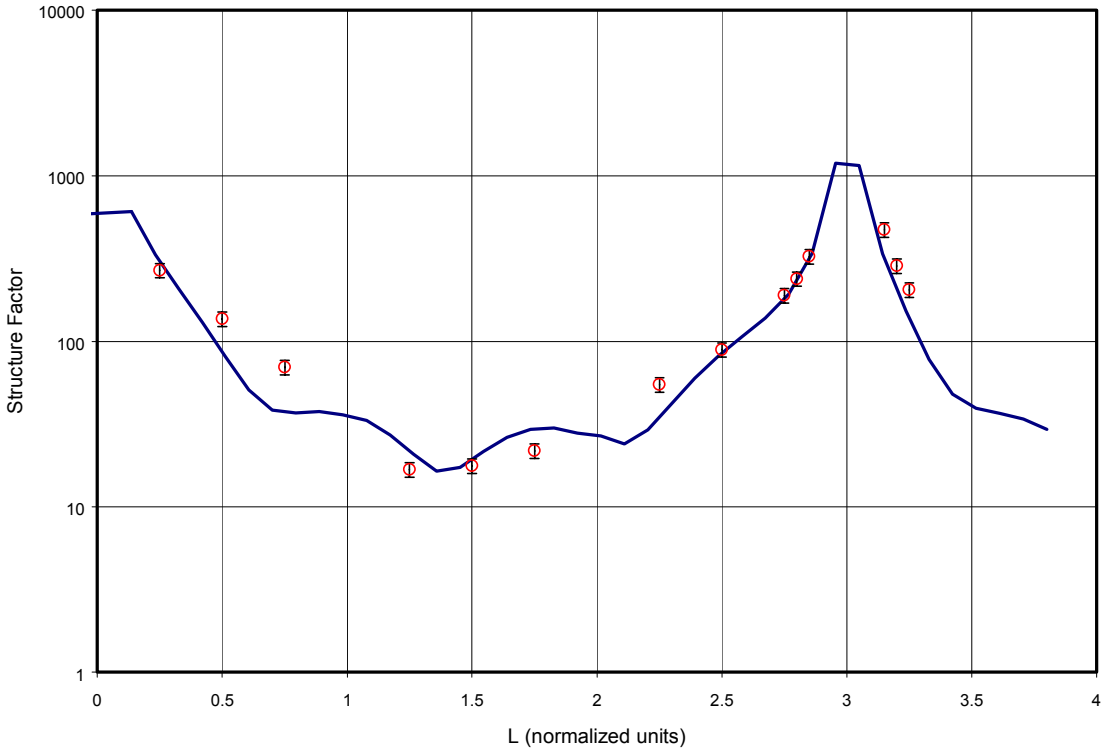

Figure 2-13 (7, 7) CTR

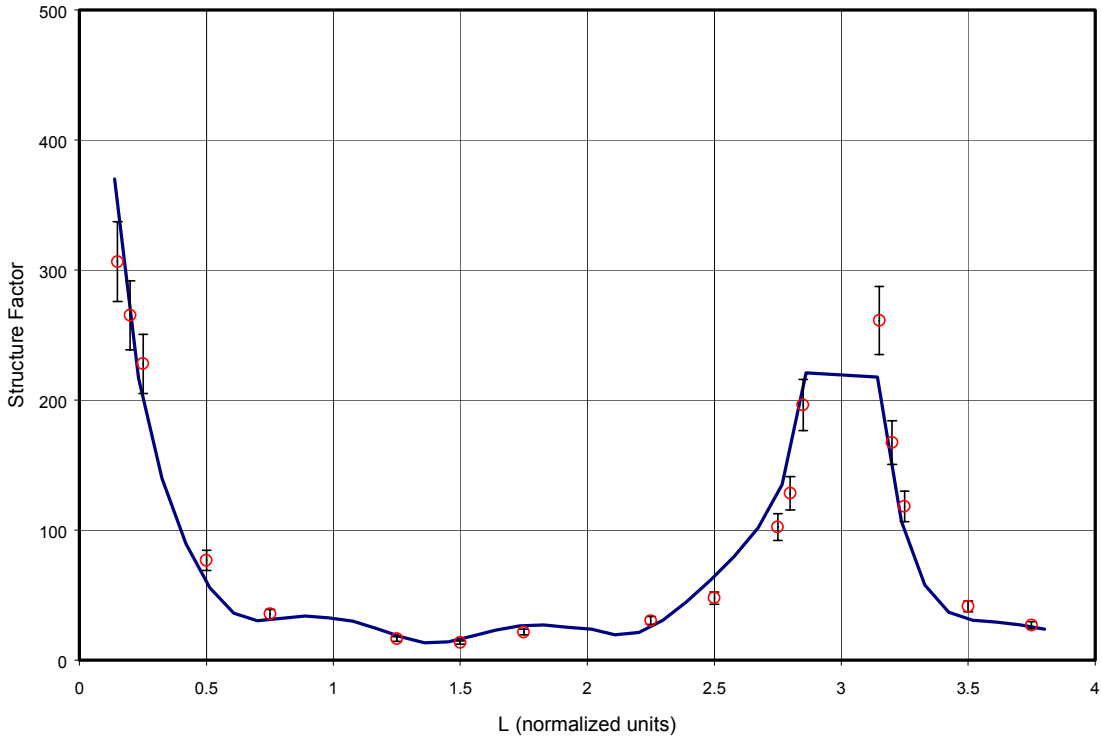

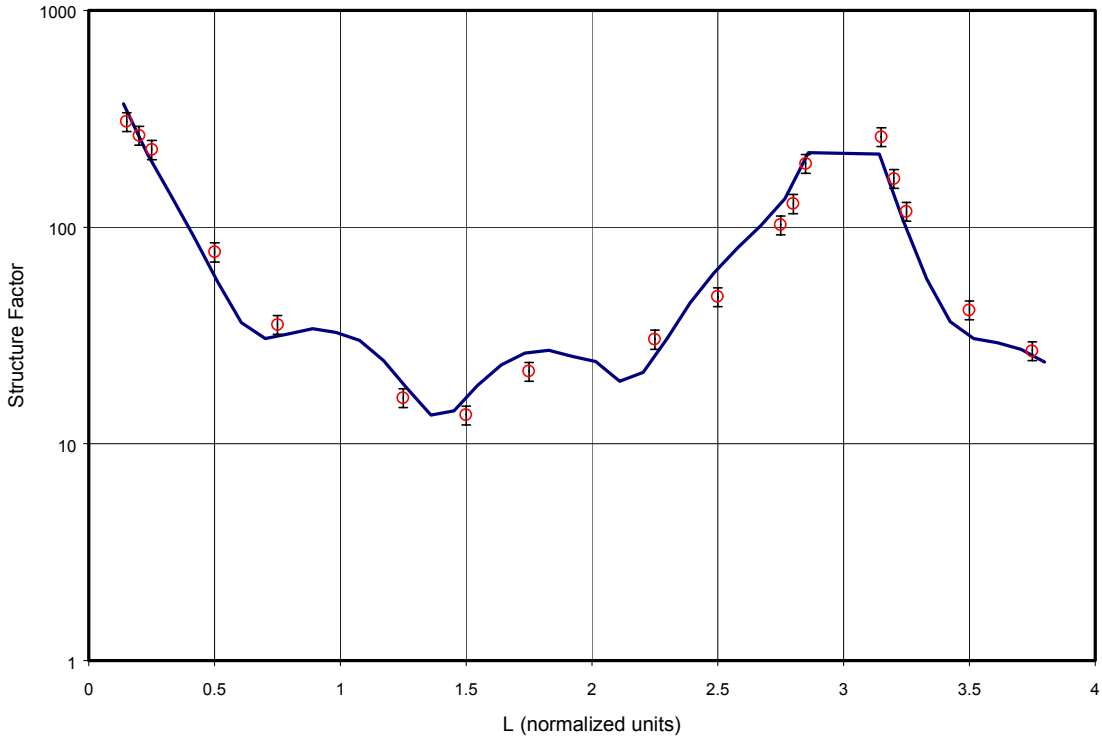

Figure 2-14 (14, 14) CTR

3 High Temperature Transition of Si7x7

3.1 History

It is often observed that below the melting point of the bulk disordering of the crystal surfaces may occur. This effect is another illustration of the fact that the dynamics between the atoms at the surface is quite different in general from that of the bulk. The two well-known modes of disordering of the surface are: surface roughening and surface melting. Surface roughening is a process of step proliferation, which results in a divergence of the height-height correlation function. Surface melting involves formation of thin quasiliquid surface layer whose thickness increases with increasing temperature and eventually diverges at the bulk melting point. Metal surfaces show such typical phase transition (ordered to disordered) with increase of temperature. On the other hand, phase transition of semiconductor (covalent) surfaces is not well understood.

The Si(111) surface has been studied intensely for scientific and technological reasons. The nature of the equilibrium low temperature (7x7) reconstruction of Si(111) was for many years an attractive yet difficult scientific puzzle; the dimer adatom stacking fault (DAS) solution of Takayanagi has served as a blueprint for many scientific studies. Over the years many different scientific techniques have been applied to enhance and better understand the DAS model. In the previous chapter a study for understanding the 3D model of the structure and effects of anharmonic inter-atomic potential on the structure was presented, using X-ray diffraction techniques. Although the structure of the surface is considered to be well understood and agreed upon at room temperature, there continues to be a dispute about the structure of the Si(111) surface at high temperatures. There is a significant amount of technological relevance and importance of this in processes such as surface reaction and film growths.

The Ge(111) happens to be one of the few semiconductor surfaces whose structural transition and high temperatures has been studied intensively. It was shown by McRae that the disordering of the surface of Ge(111) happens about

160K below the bulk melting point. This disordering is confined to the topmost bilayer till the temperature reaches the proximity of the melting point. This mode of melting where the disordering is limited to the first bilayer is called incomplete surface melting. The structural similarity between Ge and Si leads one to imagine that Si(111) surface would demonstrate very similar behavior. Recent RHEED (reflection high energy electron diffraction) and HAS (helium atom scattering) have shown that the surface of Si(111) transitions to a disordered state at 1470K, well below the melting point of Si.

Apart from the disordering of the surface at around 1470K the Si(111) surface shows another transition in the temperature range 1110-1140K. In this structural phase transition the 7x7 reconstruction of the Si(111) is lost and gives rise to a 1x1 reconstructed phase. In this chapter we investigate the high temperature ordered state of Si(111).

3.2 High Temperature Phase of Si(111)

The reversible transition of Si(111) 7x7x to a 1x1 phase at around 1120K was first reported by Lander in 1964. In the LEED and RHEED experiments the 7x7 super-lattice peaks disappear continuously over a temperature Range of ~50K. These observations lead to the question of whether the transition is first order or second order (in violation of Landau symmetry rule). Recent STM studies have shown the co-existence of the 7x7 and 1x1 around T_c phase strongly indicating this to be a first order transition. There exists considerable amount of disputed regarding the nature of the surface above this transition temperature whereas almost all the studies unanimously show that the 7x7 structure is lost. STM measurement of adatom trapping by quenching the 1x1 phase to below T_c indicates a 2x2 distribution (partially disordered) over the truncated 1x1 surface. Studies by Phaneuf and WIilliams indicate the presence of a broad half-ordered peak. The presence of such a peak indicate the presence of the adatoms on a 2x2 lattice but the broad nature of the peak is attributed to the fact that this layer of adatoms contains certain degree of disorder. The presence of adatoms helps in reducing trhe number of dangling bonds thus

decreasing the surface energy of the 1x1 phase. In this study we show the presence of a ~0.25 monolayer of adatoms in the 1x1 phase and some other interesting features that explain the transition from the room temperature 7x7 phase to the high temperature 1x1 phase of Si(111) surface.

3.3 Experiment

The first step towards studying the high temperature transition of Si(111) is to form a good 7x7 reconstructed structure. The experiments were conducted at X16A beamline at the National Synchrotron Light Source at the Brookhaven National Labs. This beamline has a 5-circle high-resolution diffractometer for conducting surface x-ray scattering experiments in ultrahigh vacuum. The beamline uses a bent cylindrical mirror to focus bending-magnet radiation onto a $1mm^2$ spot on the sample. The incident beam was monochromated (1.57 Å) by a pair of parallel Si(111) crystals. We used a 6mmX30mm Si(111) sample in this experiment. The sample was first etched to produce a good oxide layer (the oxide is the key to a good 7x7 reconstruction). Then it was flashed to 1200^oC for 5 seconds and cooled very quickly to about 900^oC. From this temperature the sample was slowly cooled to 750^oC. This is the temperature region where the surface forms it's ordered reconstruction. Then from 700^oC it was cooled quickly to the room temperature. The pressure in the chamber during the measurements during the next 84 hours was found to be around $5.2X10^{-10}$ torr.

The result was a partially 7x7 reconstructed SI(111) surface. Figure 3-1a and 3-1b show the crystal truncation rods (CTR) from the prepared 7x7 surface. An interesting feature of this sample was the observation of the stacking fault. This can be inferred from the small peak at L= +1 , which in a faultless sample is not a Bragg Peak. This effect of stacking fault in the bulk can be explained by figure 3-2. Consider the regular stacking sequence in the bulk to be ABCABC where A, B, and C represent each layer of the bulk unit cell.

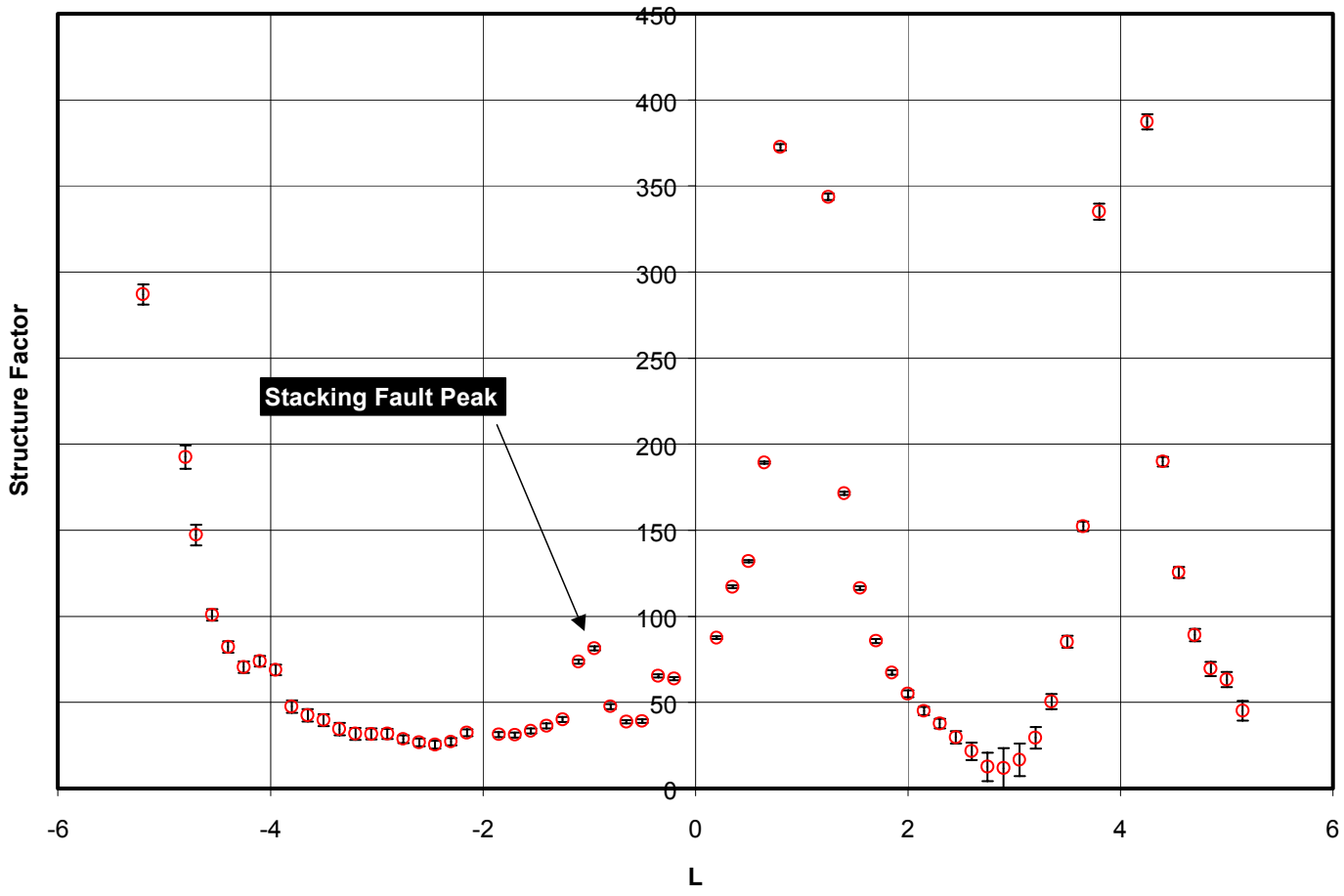

Figure 3-1 (1,0,L) CTR from 7x7 reconstruction

Consider a stacking fault resulting in the stacking sequence of ABACBACBA as shown in figure 3-2. It can be easily noticed that the stacking fault results in a stricture 180^{o} rotated in the XY plane. Thus the [h,k,l] reflection structure factor in the faulted stacking order are equivalent to the [-h,-k,l] structure factor of the unfaulted stacking order. It can be shown, using the inversion symmetry of the lattice:

$$\left|f(-\vec{q})\right|^2 = \left|\int \rho(\vec{r})\, e^{-i(-\vec{q}\cdot\vec{r})}\, d\vec{r}\right|^2 = \left|-\int \rho(-\vec{r})\, e^{-i(\vec{q}\cdot\vec{r})}\, d\vec{r}\right|^2 \quad (\vec{r} \Rightarrow -\vec{r})$$

by using the inversion symmetry of the crystal ($\rho(\vec{r}) = \rho(-\vec{r})$)

$$\left|f(-\vec{q})\right|^2 = \left|f(\vec{q})\right|^2 \quad \Rightarrow \quad F(-h,-k,l) = F(h,k,-l)$$

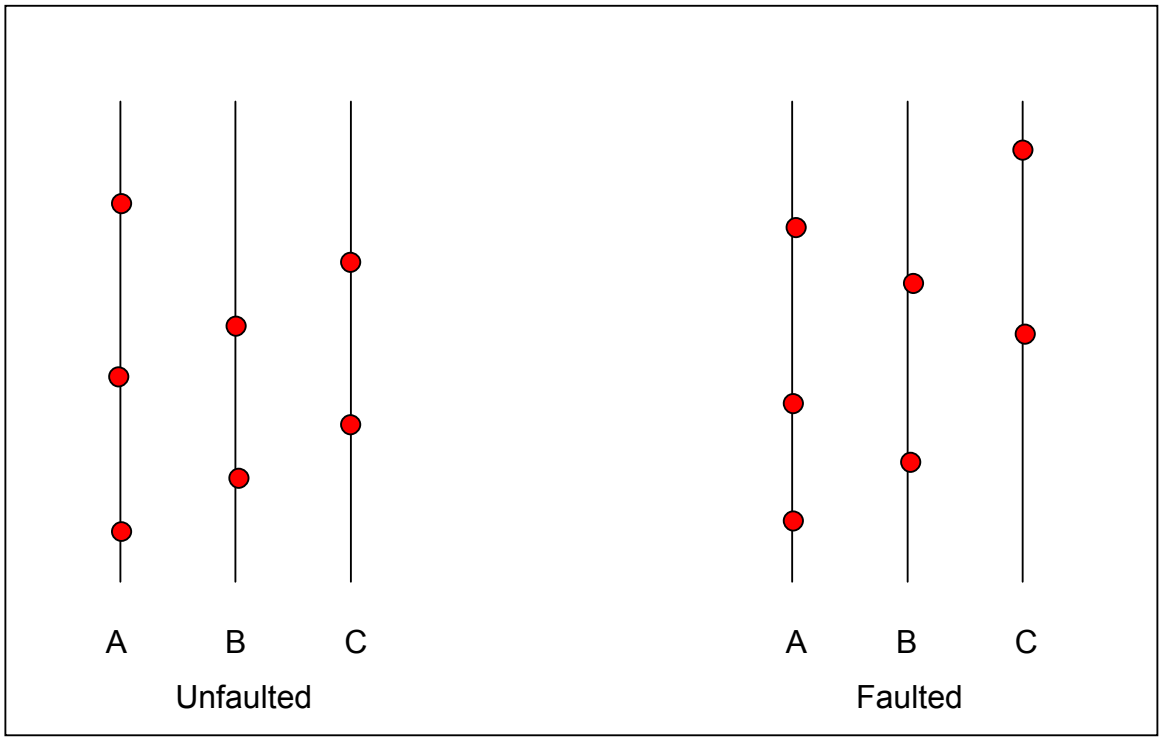

Figure 3-2 Stacking fault on Si(111)

The presence of the stacking fault in this sample is considerably higher than what was observed in the sample used in the study described in Chapter 2. This imperfection due to stacking fault can be compensated for by taking appropriate measures during data processing. In case of Si(111) the CTRs are known to have a p3m1 symmetry (same as the bulk), which makes the (1, -1) and (0, -1) CTRs symmetry equivalents of the (1,0) CTR. During data processing these three reflections are averaged together with appropriate weights counteracting any imperfections and disorders which destroys this symmetry e.g. mis-cut of the crystal, dislocations and stacking fault.

Due to the large dynamic range of the temperature 300K – 1200K in the experiment the thermal expansion of the sample was too large for the diffractometer to work with one set of orientation matrices. Orientation matrices are the location, expressed in terms of the Eularian angles of the diffractomete,

of known Bragg peaks. With help of the location of these known Bragg peaks, along with the knowledge of the wavelength of the X-ray and the lattice constants of the crystal, the diffractometer is able to calculate the Eularian angles for any location in the reciprocal space. As the temperature increases the lattice constants change which requires a new set of orientation matrices. In this experiment several sets of orientation matrices were required, each being valid only in a unique range of temperatures.

In the beginning two observation points were chosen to characterize the changes in the structure as the Si(111) transitions from the well known 7x7 reconstructed phase to the relatively unknown 1x1 phase, with increasing temperature. The first of these observation points was on the (3/7,0) rod which is one of the strongest surface order rod arising from the 7x7 reconstruction of the surface. The change in the intensity of this rod can be understood as an indication of the fraction of the surface which is 7x7 reconstructed. The observation point on this rod was chosen such that the component of the scattering vector perpendicular to the surface was as small as possible given the geometry of the experimental setup. By keeping the perpendicular component of the scattering vector as small as possible the intensity of the reflection is made insensitive to the changes parallel to the surface. Figure 3-3 shows the changes in the intensity of the reflection at this observation point. As it can be seen from the figure the strong intensity of the reflection before indicates the presence of the 7x7 reconstruction. The intensity from this reflection decreases as the temperature increases through the transition zone and finally vanishes to the background intensity. This strongly indicates that the 7x7 phase transition co-exists with 1x1 phase in the transition region before vanishing completely. The transition of the 7x7 phase happens over a finite temperature range, a strong indicator of a first order phase transition.

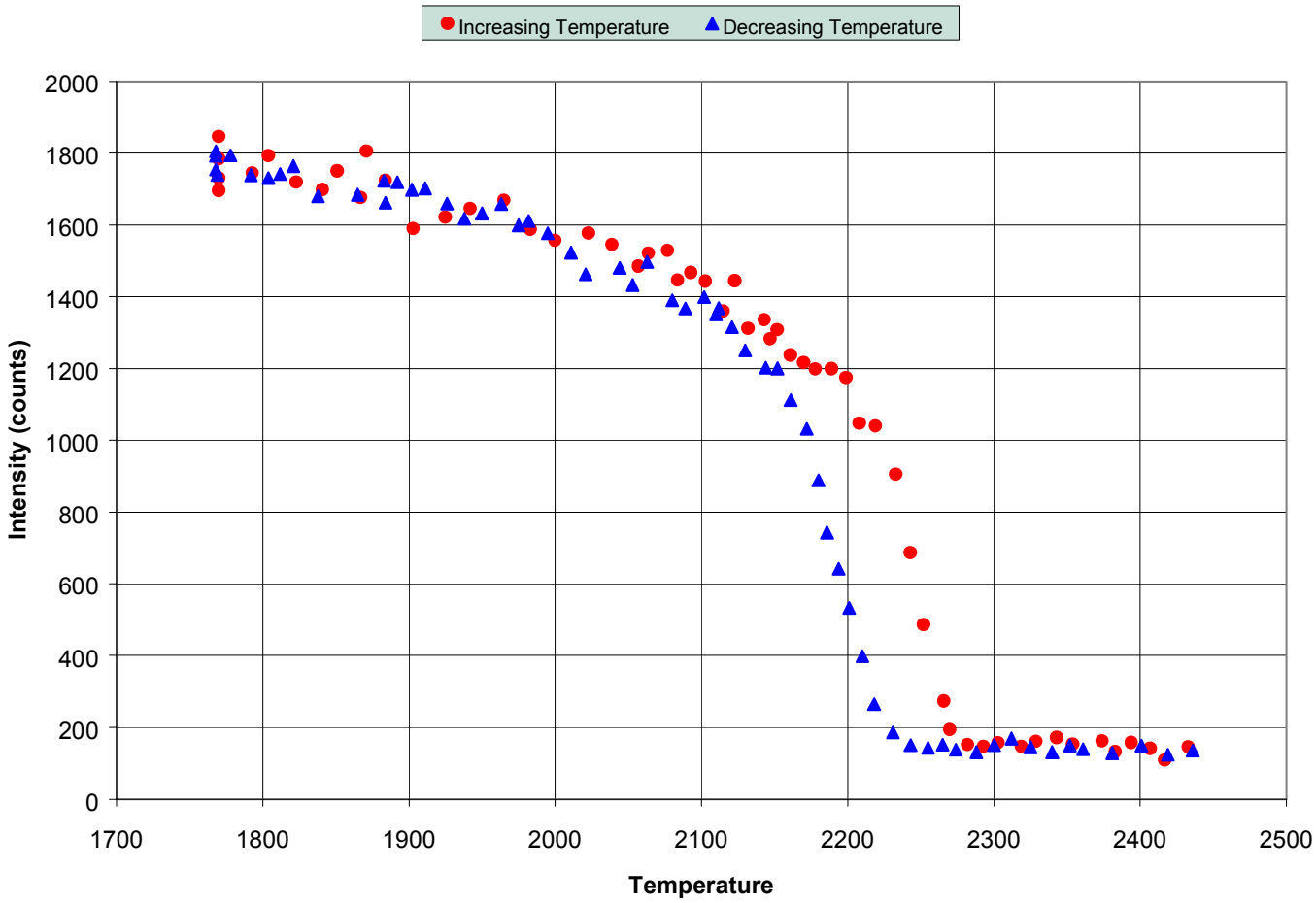

Figure 3-3 Variation of the (3/7,0,0.2) reflection

The second observation point was chosen to fall on a crystal truncation rod, away from a Bragg Peak to maximize the effect of surface transitions. Figure 3-4 shows the change in the intensity of the (1,0,2) point on the reciprocal lattice. The increase in the intensity with increasing temperature indicates that the transition includes more than mere disordering of the adatoms. It is presumed at this point that the increase in the intensity after the transition to the 1x1 state can be explained by the change in the stacking fault.

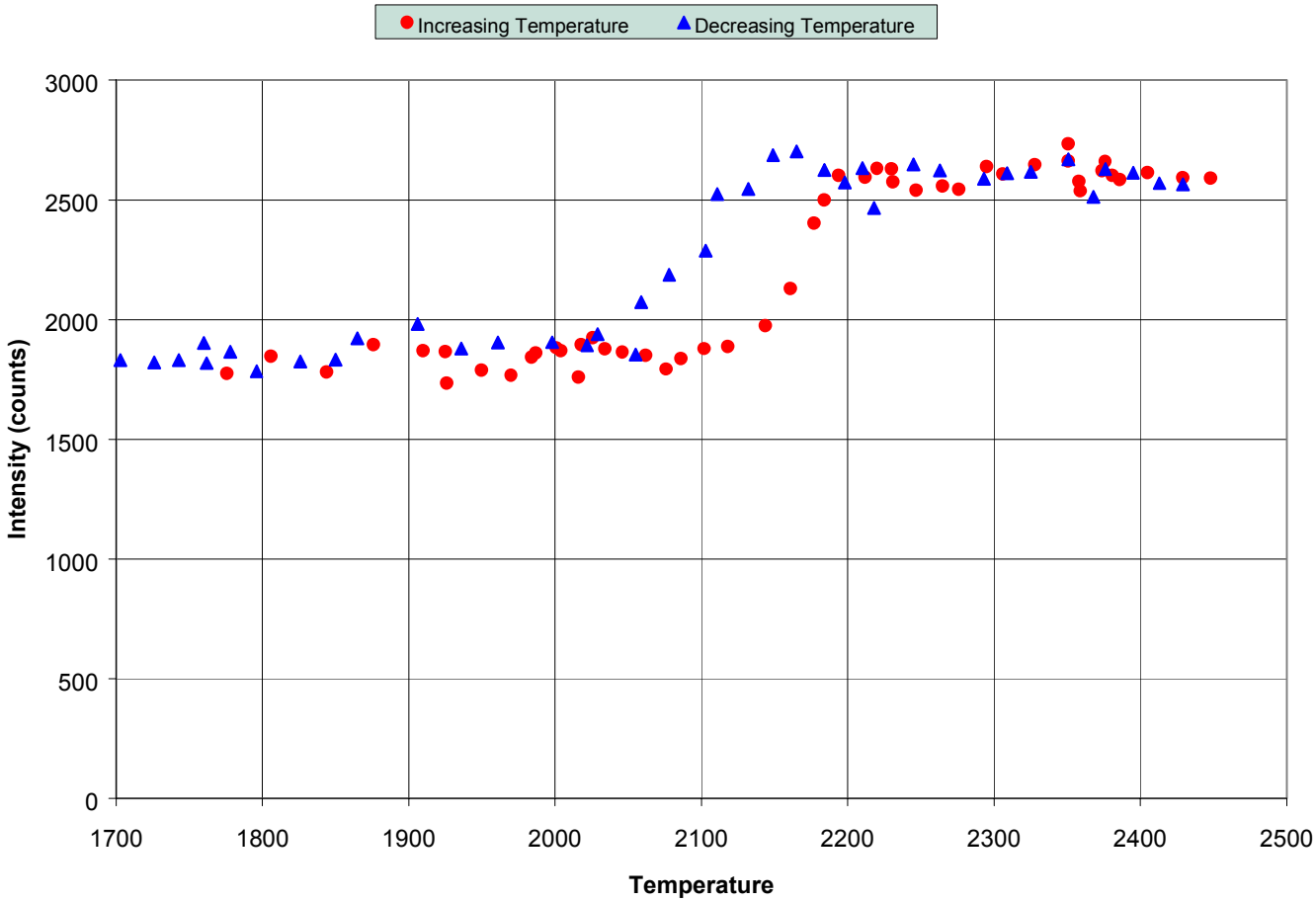

Figure 3-4 Variation of the (1,0,2) reflection

3.4 Data Analysis

It is evident from figure 3-4 that the 7x7 reconstruction of the Si(111) surface vanishes after the phase transition, hence to compare the structure before and after the transition one must focus on the CTRs which are present both before and after the transition. The CTRs depend on the 1x1 structure of the surface as shown by the equations:

$$F(\vec{q}) = F_{hkl} = \int \rho(\vec{r}) \exp(i\vec{r} \cdot (h\vec{b}_1 + k\vec{b}_2 + l\vec{b}_3)) \, d^3\vec{r}$$

where h, k, l are multiples of 7

$h = 7n_1, k = 7n_2, l = 7n_3$

The position vectors can be expressed in terms vectors 1/7th the size of the unit vectors of the 7x7 unit cell, i.e.

define new vectors d_1, d_2, d_3 such that

$d_1 = a_1 / 7$

$d_2 = a_2 / 7$

$d_3 = a_3 / 7$

The position vector can be expressed as:

$\vec{r} = (i_1 + f_1)\vec{d}_1 + (i_2 + f_2)\vec{d}_2 + (i_3 + f_3)\vec{d}_3$, where i_1, i_2, i_3 are integers and f_1, f_2, f_3 are fractions. The structures factor for the CTR can be expressed as

$$F(\vec{q}) = \int \rho(\vec{r})\, \exp(i\vec{r} \cdot \vec{q})\, d^3\vec{r}$$

$$= \int \rho((i_1 + f_1),(i_2 + f_2),(i_3 + f_3))\, \exp(2\pi i(f_1 n_1 + f_2 n_2 + f_3 n_3))\, df_1\, df_2\, df_3$$

Thus the structure factor depends only on the fractional part (f_1, f_2, and f_3) of the representation of the position vector in units of d_1, d_2, and d_3. This can be also interpreted as the unit cell (a_1 X a_2 X a_3) being folded back into the 1/7 unit cell (d_1 X d_2 X d_3). For a 7x7 reconstructed surface this means that the CTR depends only on the entire 7x7 unit cell folded back into the 1x1 unit cell. This result helps us to define only the 1x1 folded structure to calculate the CTRs both before and after the transition.

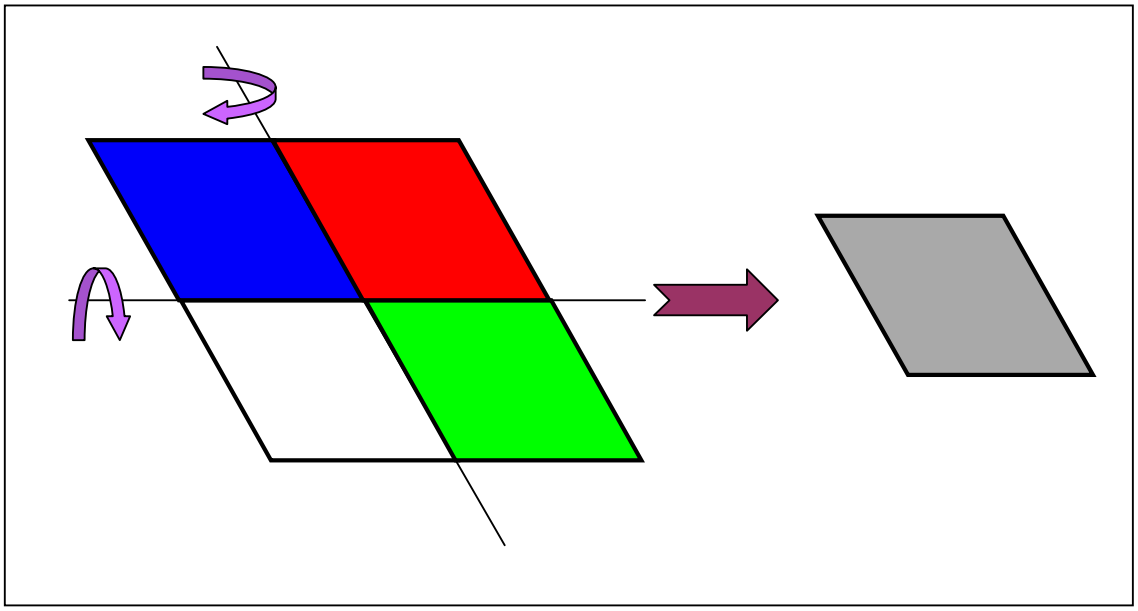

Figure 3-5 Folding the 2x2 structure onto the 1x1

Figure 3-5 shows the representation of folding a 2x2 structure on the 1x1 basic structure. The folding of the 7x7 structure onto the 1x1 involves similar, but many more such operations. As mentioned earlier this operation allows one to define the entire 7x7 structure (or any other reconstruction) on the 1x1 unit cell. However simple this may sound it is important to define the all the aspects of the 7x7 reconstruction onto the 1x1 unit cell. For example a 1x1 unit cell has an atom at the location (2/3, 2/3, 0.5833) (in 1x1 units) but in the representation of the 7x7 unit cell this location is shared between the dimers and regular Si atoms. At the location (2/3, 2/3, 0.5833), in the representation of the 7x7 unit cells, there are 3 dimers and one regular atom. The dimers and the regular atom are coupled to

Name		X	Y	Z	Occupation
Adatoms	Si	0.66667	0.66667	0.92267	0.25
Trimers (faulted)	Si	0	0	0.66667	0.166666667
Trimers (faulted)	Si	0	0	0.66667	0.166666667
Trimers (faulted)	Si	0	0	0.66667	0.166666667
Trimers (unfaulted)	Si	0.33333	0.33333	0.66667	0.166666667
Trimers (unfaulted)	Si	0.33333	0.33333	0.66667	0.166666667
Trimers (unfaulted)	Si	0.33333	0.33333	0.66667	0.166666667
Lyr 2 (regular)	Si	0.66667	0.66667	0.58333	0.375
Lyr 3 (regular)	Si	0.66667	0.66667	0.33333	0.75
Lyr 2 (Dimers)	Si	0.66667	0.66667	0.58333	0.0625
Lyr 2 (Dimers)	Si	0.66667	0.66667	0.58333	0.0625
Lyr 2 (Dimers)	Si	0.66667	0.66667	0.58333	0.0625
Lyr 2 (Dimers)	Si	0.66667	0.66667	0.58333	0.0625
Lyr 2 (Dimers)	Si	0.66667	0.66667	0.58333	0.0625
Lyr 2 (Dimers)	Si	0.66667	0.66667	0.58333	0.0625
Lyr 2 (below adatoms)	Si	0.66667	0.66667	0.58333	0.25
Lyr 3 (below adatoms)	Si	0.66667	0.66667	0.33333	0.25
Lyr 4	Si	0	0	0.25	1

Table 3-1 7x7 reconstruction in 1x1 unit cell

different displacement parameters. Table 3-1 shows this representation of the 7x7 unit cell.

Each of these atoms is coupled to a displacement vector, which also happen to be the fitting parameters. The two CTRs analyzed in this study are (1,0,l) and (1,1,l) which happen to be two of the strongest CTRs form the Si(1x1) surface and have the strongest contribution from the 7x7 reconstruction as seen in the previous chapter. The starting points for the displacement parameters were the results form the room temperature 3D study of the 7x7 by reconstruction. Due to lack of extensive data the horizontal displacements were kept fixed and only the out of plane displacement parameters were varied. A large change in the Debye-Waller factors were observed. Figure 3-6 shows the change in the (1,0,l) CTR before and after the transition.

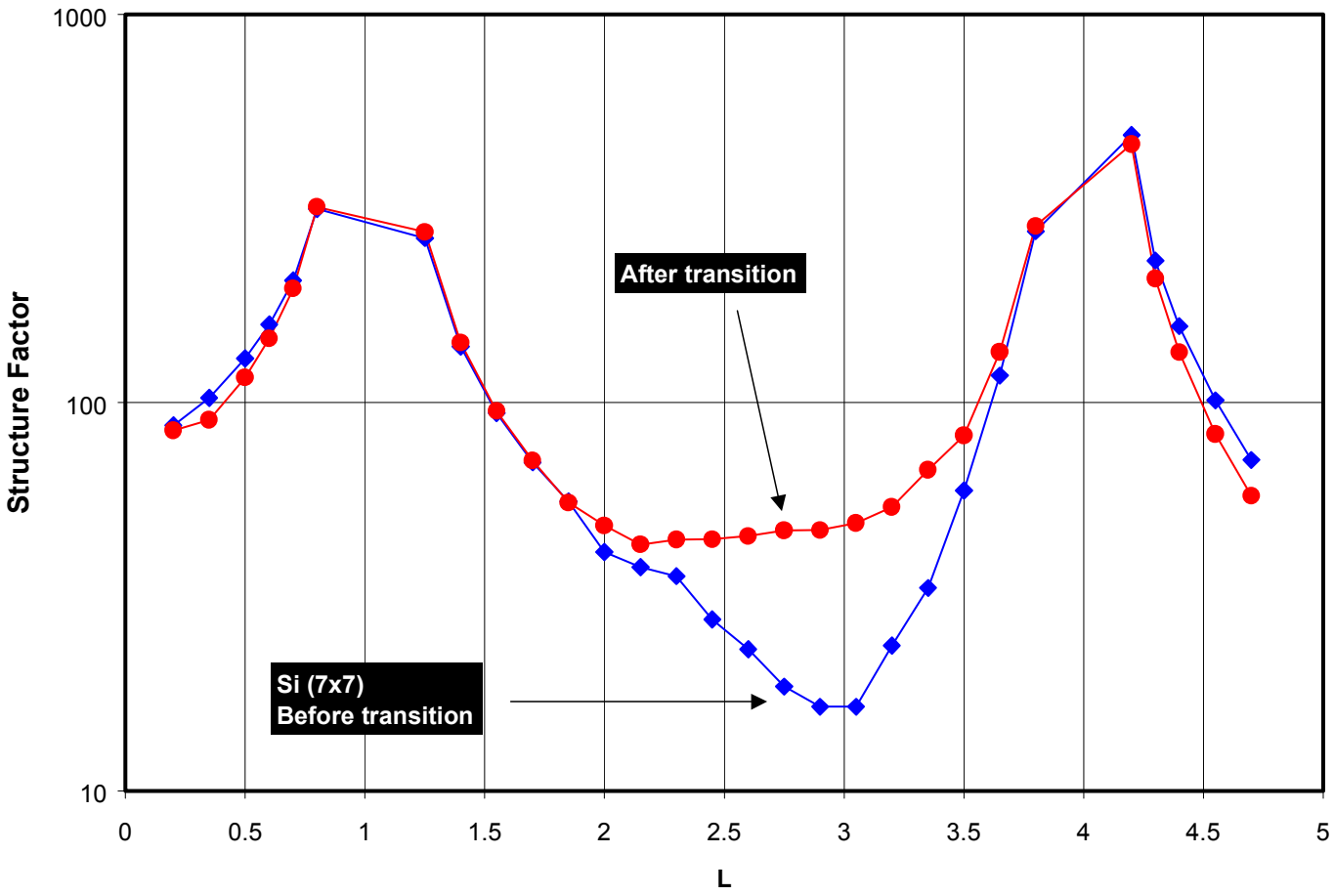

Figure 3-6 (1,0,L) CTR before and after the transition

As expected the changes in the CTR are, before and after the transition, are most observable between the Bragg peaks where the contribution from the bulk is minimum. One of the interesting change in the profile of the (1,0,l) CTR is around l = 3, where the deep valley vanishes after the transition. In case of Si7x7 this valley is attributed to the stacking fault. As mentioned in the previous chapter the stacking fault arises as the surface tries to minimize stress. The stacking fault reduces the stress by decreasing the number of atoms in a layer. The contraction of the trimer chain around the adatom is another such mechanism by which the Si7x7 surfaces reduces the stress.

From previous studies it has been shown that at these temperatures the adatoms are present and reduce the surface energy by decreasing the number of dangling bonds. However since the deep valley , which is attributed to the stacking fault vanishes we suspect that the stacking fault vanishes after the transition giving

Adatoms	Si	0.833331667	0.833331667	0.83467
Lyr 1	Si	0.166665	0.166665	0.66667
Lyr1	Si	0.666665	0.166665	0.66667
Lyr1	Si	0.166665	0.666665	0.66667
Lyr1	Si	0.666665	0.666665	0.66667
Lyr2	Si	0.333335	0.333335	0.58333
Lyr2	Si	0.833335	0.333335	0.58333
Lyr2	Si	0.333335	0.833335	0.58333
Lyr2	Si	0.833335	0.833335	0.58333
Lyr3	Si	0.333335	0.333335	0.33333
Lyr3	Si	0.833335	0.333335	0.33333
Ly3	Si	0.333335	0.833335	0.33333
Ly3	Si	0.833335	0.833335	0.33333
Lyr4	Si	0	0	0.25
Lyr4	Si	0.5	0	0.25
Ly4	Si	0	0.5	0.25
Ly4	Si	0.5	0.5	0.25

Table 3-2 Si(111) unit cell with a 2x2 grid of adatoms

rise to double layer truncated Si(111) surface with a 2x2 grid of adatoms on top of it. Table 3-2 shows this unfaulted double layer terminated SI(111) surface with

a adatoms. We refer to this structure as the 2x2 structure. This model is assumed to represent the structure of the surface after the transition and is fitted to the (1,0,l) and the (1,1,l) CTR.

To justify the rationale for this assumption (vanishing of the stacking fault) we show calculated results for the (1,0,l) CTR of a double layer terminated SI(111) surface with a variable degree of stacking fault. The most important feature is the vanishing of the valley at L ≈ 3.

Figure 3-7 (1,0,l) Calculated CTR with variable stacking fault

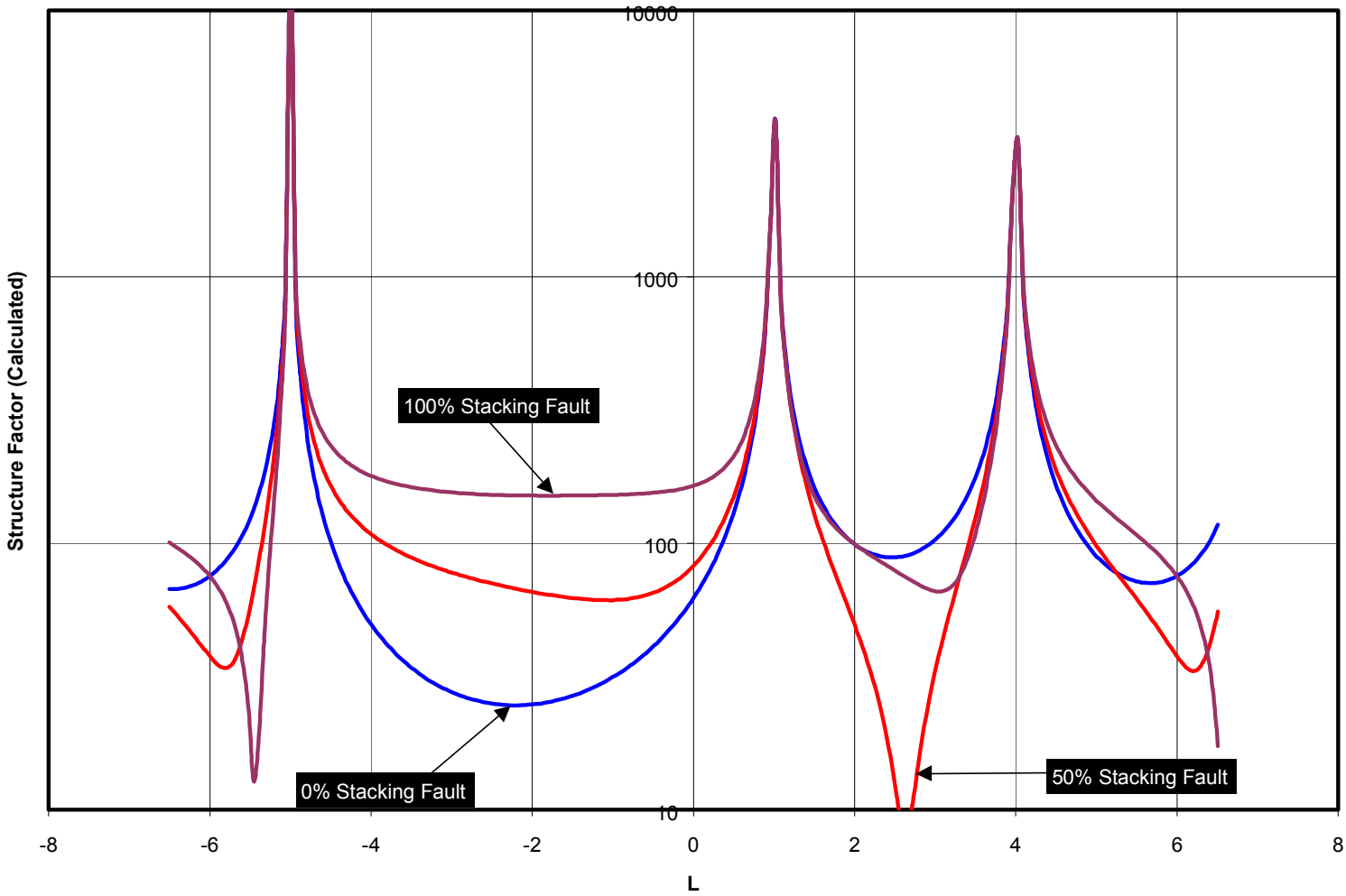

3.5 Results and Conclusions

We start the data analysis by fitting the 7x7 data before the transition. Most of the parameters were kept the same as obtained from the previous chapter. The position of the adatoms and the first layer were allowed to relax in the perpendicular direction.

The Debye-Waller factors for these atoms were also treated as fitting parameters. A considerable increase in the Debye-Waller factors was seen compared to the room temperature. Figure 3-8, 3-9 and table3-3 show the results of this fit.

The inplane relaxation of dimers and trimers were taken from our previous fit if 7x7	
Overall Scale Factor	9.82344
Roughness	0.3013
Surface Fraction	0.9556
Out of Plane relaxations (Å) (Debye-Waller Factor)	
Adatoms	0.909 (6.34)
Atoms Below Adatoms	-0.474 (3.29)

Table 3-3 Fit of Si7x7 before transition

The parameters were obtained by minimizing the chi-square (χ^2) between the observed structure factors and calculated structure factors at the data points. The best fit (as shown in table 3-3) has $\chi^2 = 3.2$. Though the fit is good the relatively large χ^2 is because of the small error bars. The 2x2 fit model with adatoms was fitted to the CTR data after the transition. Figure 3-10 and 3-11 show the fitted (1,0,l) and (1,1,l) CTR data. The good fit of the 2x2 model without stacking fault indicates that the stacking fault vanishes after the phase transition.

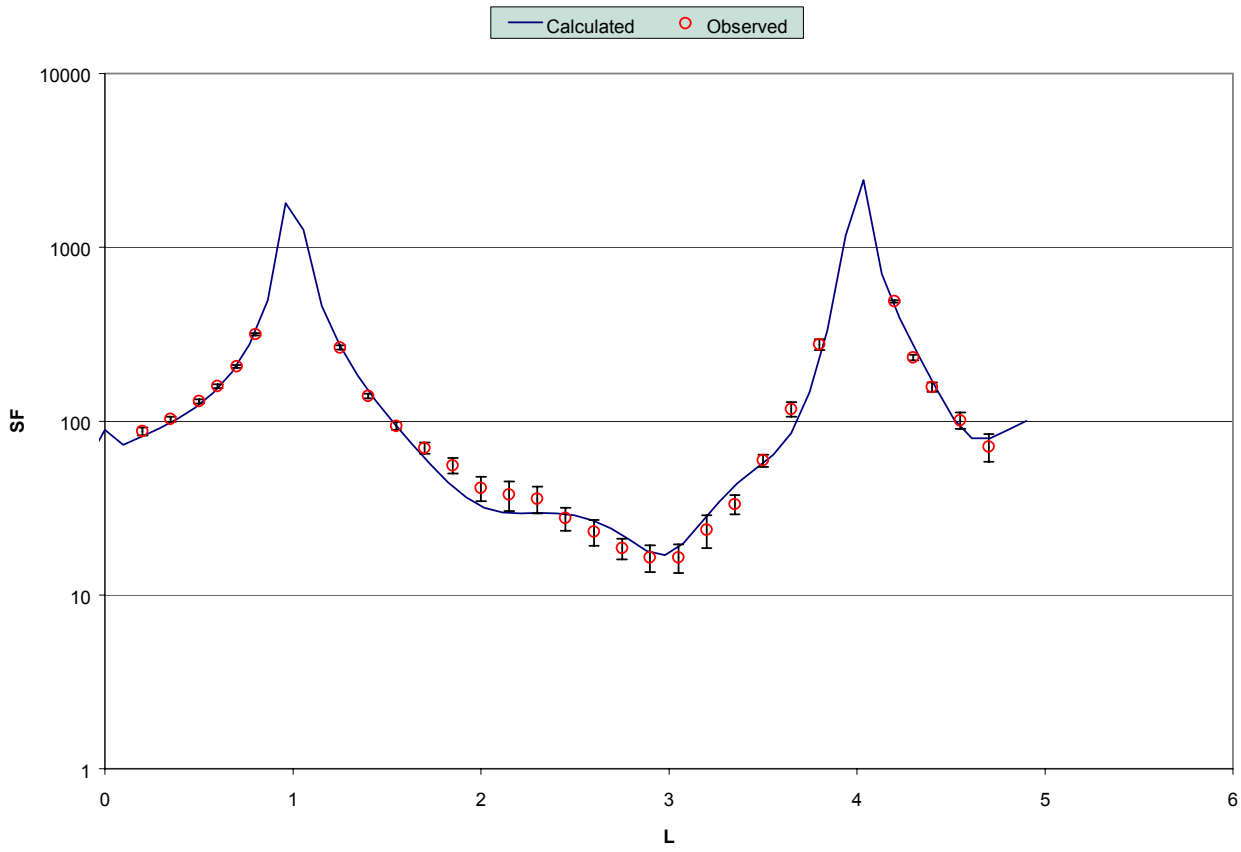

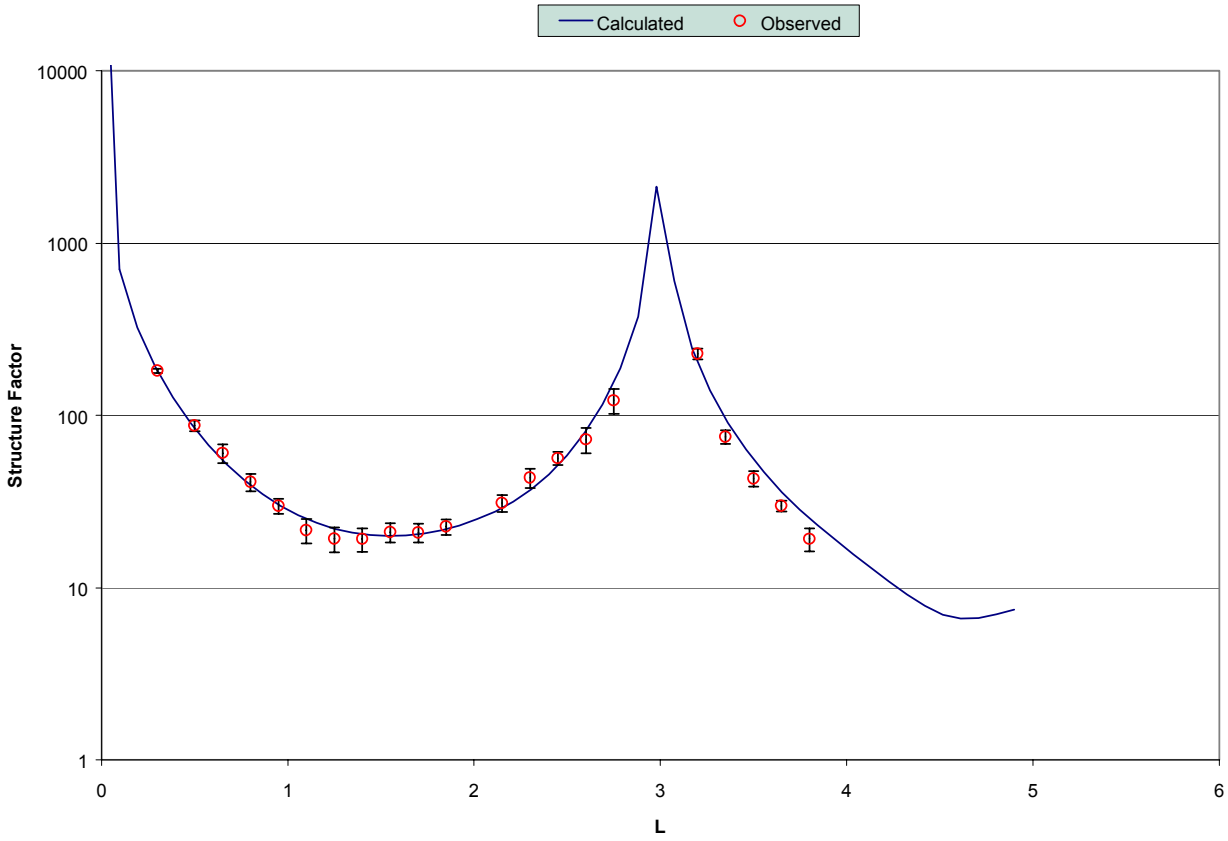

Figure 3-8 (1,1,l) CTR before transition

The stacking fault as mentioned earlier reduces the surface stress by decreasing the number atoms in each layer. As the temperature of the substrate is increased the stress on the surface is reduced due to the thermal expansion. As the temperature reduces the stacking fault is no longer required as a stress reducing mechanism. From the behavior of the CTRs we conclude that after the phase transition the stacking fault disappears. However the adatoms are still present forming a 2x2 structure which reduces the of dangling bonds at the surface. The data from the CTR is insufficient to conclude whether the adatoms are ordered or disordered. To answer that question one needs to look for the 2x2 surface rods. If the adatoms are ordered then one can safely asssume the presence of the 2x2 order surface rods as shown in figure 3-10. The surface rods would be absent however, if the adatoms were disordered.

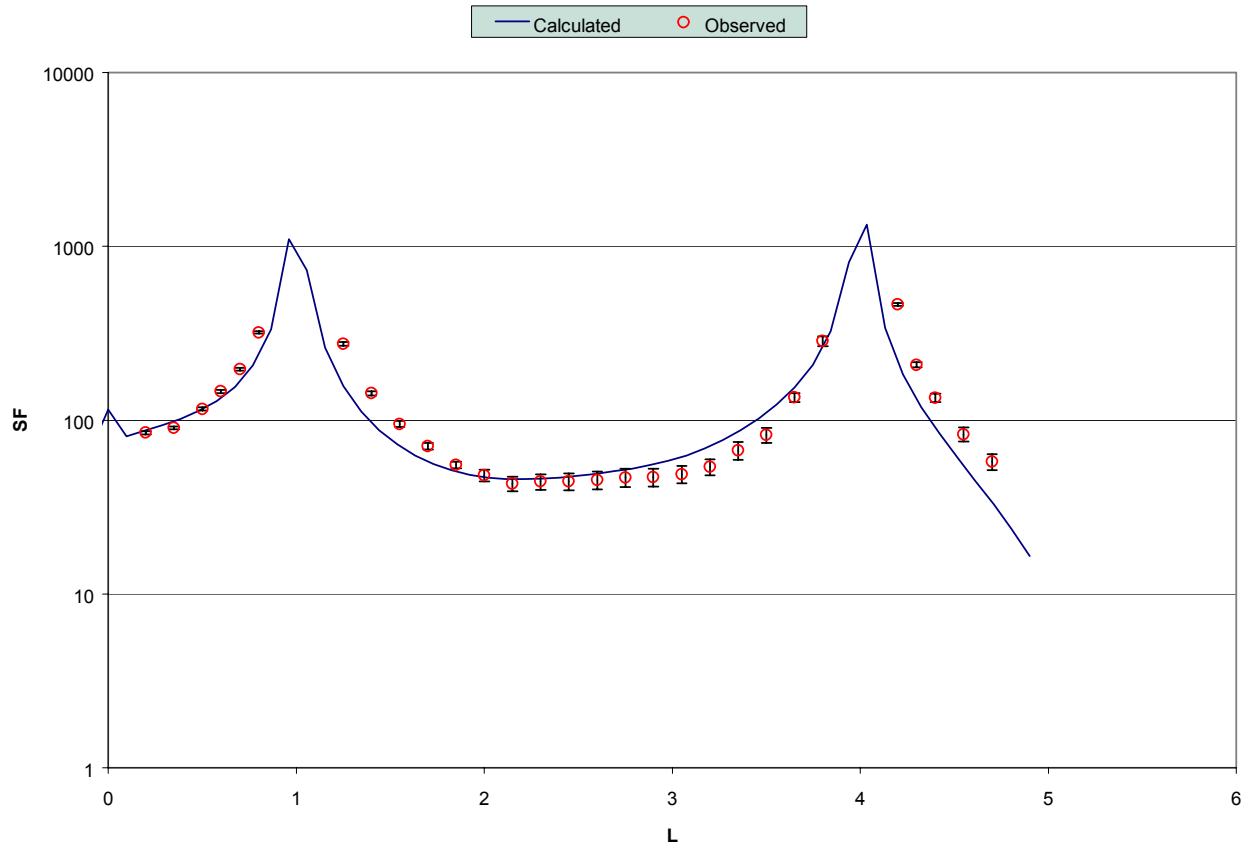

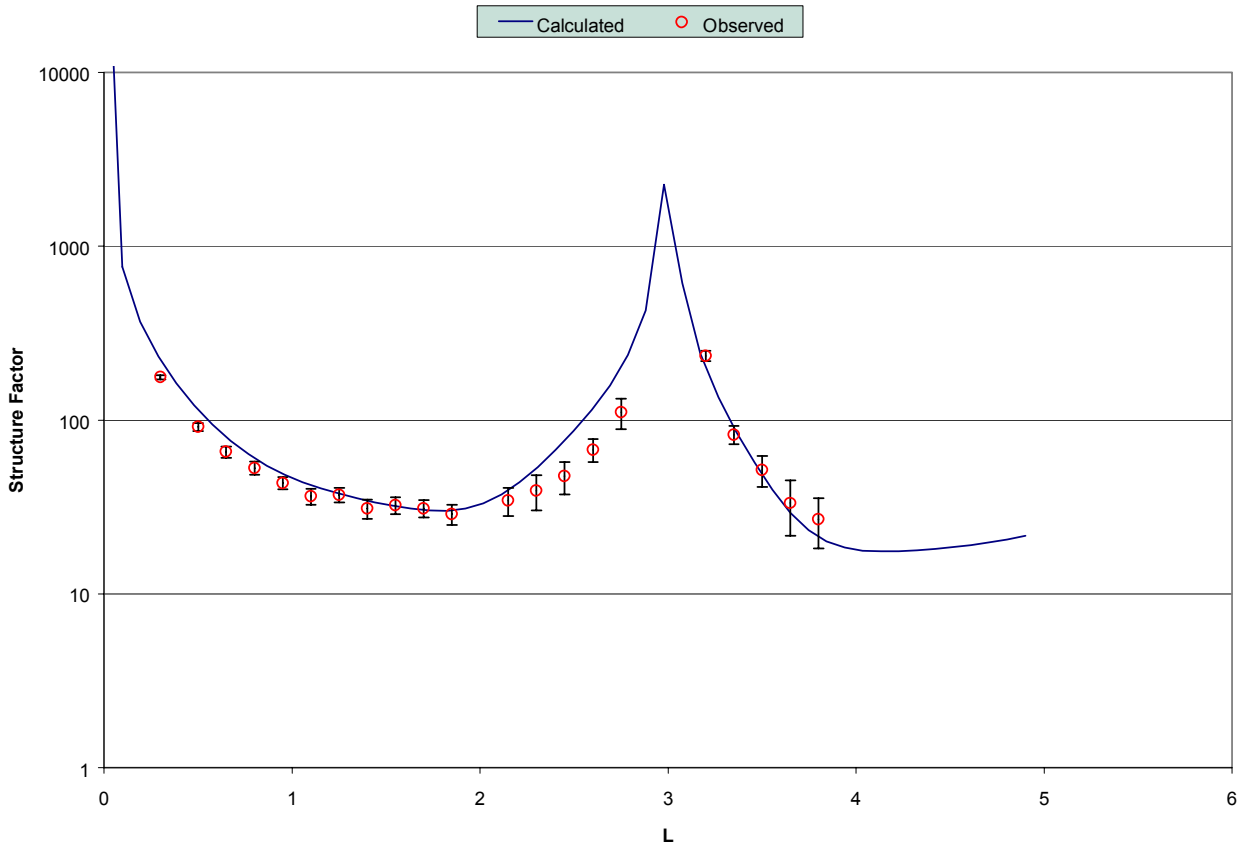

Figure 3-9 (1,0,l) & (1,1,l) CTR after transition